Advances in Water Resources 106 (2017) 95–110

Contents lists available at ScienceDirect

Advances in Water Resources

journal homepage: www.elsevier.com/locate/advwatres

Quasi-steady state conditions in heterogeneous aquifers during pumping tests

Yuanyuan Zha[a,g], Tian-Chyi J. Yeh[b,h], Liangsheng Shi[a], Shao-Yang Huang[f], Wenke Wang[e], Jet-Chau Wen[c,d,*]

[a] State Key Laboratory of Water Resources and Hydropower Engineering Science, Wuhan University, Wuhan, China
[b] Department of Hydrology and Atmospheric Sciences, University of Arizona, Tucson, AZ, USA
[c] Department of Safety, Health and Environmental Engineering, National Yunlin University of Science and Technology, Touliu, Yunlin, Taiwan
[d] Research Center for Soil and Water Resources and Natural Disaster Prevention, National Yunlin University of Science and Technology, Touliu, Yunlin, Taiwan
[e] Key Laboratory of Subsurface Hydrology and Ecological Effects in Arid Region, Chang'an University, Xi'an, China
[f] Graduate School of Engineering Science and Technology, National Yunlin University of Science and Technology, Douliou, Taiwan
[g] Key Laboratory for Groundwater and Ecology in Arid and Semi-Arid Areas, China Geological Survey, Xi'an, China
[h] Key Laboratory for Water Environment and Resources, Tianjin Normal University, Tianjin, China

ARTICLE INFO

Article history:
Received 29 May 2016
Revised 14 March 2017
Accepted 22 March 2017
Available online 24 March 2017

Keywords:
Ergodicity
Quasi-steady
Stochastic analysis
Pumping

ABSTRACT

Classical Thiem's well hydraulic theory, other aquifer test analyses, and flow modeling efforts often assume the existence of "quasi-steady" state conditions. That is, while drawdowns due to pumping continue to grow, the hydraulic gradient in the vicinity of the pumping well does not change significantly. These conditions have built upon two-dimensional and equivalent homogeneous conceptual models, but few field data have been available to affirm the existence of these conditions. Moreover, effects of heterogeneity and three-dimensional flow on this quasi-steady state concept have not been thoroughly investigated and discussed before. In this study, we first present a quantitative definition of quasi-steady state (or steady-shape conditions) and steady state conditions based on the analytical solution of two- or three-dimensional flow induced by pumping in unbounded, homogeneous aquifers. Afterward, we use a stochastic analysis to investigate the influence of heterogeneity on the quasi-steady state concept in heterogeneous aquifers. The results of the analysis indicate that the time to reach an approximate quasi-steady state in a heterogeneous aquifer could be quite different from that estimated based on a homogeneous model. We find that heterogeneity of aquifer properties, especially hydraulic conductivity, impedes the development of the quasi-steady state condition before the flow reaching steady state. Finally, 280 drawdown-time data from the hydraulic tomographic survey conducted at a field site corroborate our finding that the quasi-steady state condition likely would not take place in heterogeneous aquifers unless pumping tests last a long period.

Research significance

(1) Approximate quasi-steady and steady state conditions are defined for two- or three-dimensional flow induced by pumping in unbounded, equivalent homogeneous aquifers. (2) Analysis demonstrates effects of boundary condition, well screen interval, and heterogeneity of parameters on the existence of the quasi-steady, and validity of approximate quasi-steady concept. (3) Temporal evaluation of information content about heterogeneity in head observations are analyzed in heterogeneous aquifer. (4) 280 observed drawdown-time data corroborate the stochastic analysis that quasi-steady is difficult to reach in highly heterogeneous aquifers.

1. Introduction

Multi-scale heterogeneity of aquifers is the rule rather than the exception. Nevertheless, widely-accepted analyses of cross-hole pumping tests adopt an equivalent homogeneous conceptual model (Yeh et al., 2015b) to homogenize aquifer heterogeneity. Using a stochastic analysis, Wu et al. (2005) showed that the governing equation for the equivalent homogeneous model is an ensemble mean equation, embedding with effective transmissivity and storage coefficient. As such, it represents the physical principle governing the average flow over many possible realizations (i.e., an ensemble) of flow fields under the same stress, and it predicts

* Corresponding author.
E-mail address: wenjc@yuntech.edu.tw (J.-C. Wen).

http://dx.doi.org/10.1016/j.advwatres.2017.03.017
0309-1708/

ensemble mean hydraulic head fields (Yeh et al., 2015b). As a result, as one applies this model to a real-world aquifer, one inevitably invokes the ergodicity assumption (i.e., the ensemble average is equivalent to the spatial average (Sanchez-Vila and Tartakovsky, 2007)). Specifically, the predicted mean heads at a given radial distance from the pumping well will be equivalent only to the averages of heads at different locations at the same radial distance in a heterogeneous aquifer. Wu et al. (2005) subsequently advocated that using observed drawdown-time data at one observation well in an equivalent homogeneous model to estimate aquifer properties is tantamount to comparing apples and oranges. They further showed that the estimated aquifer properties from Theis solution (Theis, 1935) or Cooper and Jacob's approach (Cooper and Jacob, 1946) using one well hydrograph are ambiguously averaged properties over the cone of depression. More specifically, rather than the average values of aquifer properties over the cone of depression, the transmissivity estimate based on late time drawdown data is heavily influenced by the heterogeneity near the pumping well and the observation well, and the storage coefficient estimate is mainly related to the heterogeneity between the pumping well and the observations.

Results of analysis of data from field experiments in Huang et al. (2011), Straface et al. (2007) and Wen et al. (2010) corroborated the findings by Wu et al. (2005). They further suggested that the estimated parameters using an equivalent homogeneous model are scenario-dependent: they vary with duration of the pumping and the location of the pumping well. Yeh et al. (2015b) and Yeh and Lee (2007) pointed out that the non-intrinsic natures of these estimates mainly arise from our ignorance of the ergodicity assumption behind the equivalent homogeneous models. That is, the flow itself must sample sufficient heterogeneity in the aquifer such that the ensemble mean equation is applicable. In addition to insufficient data, the basic assumption (i.e., the form of the equivalent model) may also involve uncertainty. For instance, the selection of single-porosity or dual-porosity model may have significant impact on the equivalent parameter (especially storage coefficient) as well as the scale to reach ergodicity condition (Pedretti et al., 2016). For this reason, Yeh and Lee (2007) emphasized the necessity of detailed characterizations of the spatial distributions of hydraulic properties in order to minimize these problems.

Similar to the homogeneity assumption, quasi-steady state assumption has been widely accepted and employed in the analysis of aquifer tests. For example, the well-known Thiem equation (Thiem, 1906) assumes the existence of an effective area of inference during a pumping test and suggests the use of steady state solution to estimate hydraulic conductivity. It is also common to assume the establishment of quasi-steady flow near the pumping well during tracer tests, so that the solute transport can be studied analytically or numerically under steady velocity field [e.g., (Lu and Stauffer, 2012; Pedretti and Fiori, 2013)]. Heath and Trainer (1968) stated that if quasi-steady state conditions (called steady-shape conditions) apply to near the well, Thiem equation is applicable. Butler (1988) pointed out that steady-shape conditions are reached when $t = 100r^2S/(4T)$, where r is the distance between the pumping well and observation well, S is the storage coefficient, and T is the transmissivity. More recently, Bohling et al. (2002, 2007) and Hu et al. (2011) championed the robustness of this assumption for cutting down computational costs in analyzing hydraulic tomography (HT). The importance of steady-shape conditions in practice was reemphasized by Heath (2009). For practical modeling applications, Domenico and Schwartz (1998) proposed an aquifer system time constant for aquifer. They claimed that if the time at which we wish to observe the system is much larger than the time constant, the system will appear to be at steady state, and the system can be simulated using a steady-state model. Based on this suggestion, Anderson et al. (2015) discussed one groundwater modelers' fundamental decision—where a transient model is needed. They stated that since steady-state models are much easier to operate than transient models, the formers are typically preferred provided they adequately address the modeling objective.

By assuming existence of quasi-steady conditions in a statistically homogeneous and horizontally isotropic aquifer, Neuman et al. (2004) proposed a graph method to estimate the geometric mean, integral scale and variance of the log transmissivity field on the basis of quasi-steady data when a randomly heterogeneous, two-dimensional aquifer is pumped at a constant rate. Using numerical experiments, they showed that the mean and integral scale can be reasonably recovered if there were sufficient observations, but it was difficult to obtain accurate variance value. Neuman et al. (2007) showed the existence of quasi-steady regime in heterogeneous aquifer with numerical experiment and field data. Nevertheless, Vasco and Karasaki (2006) argued that in heterogeneous media, the onset of quasi-steady conditions might be delayed by the presence of low-conductivity regions, which fail to equilibrate with the surrounding medium.

The accuracy or validity of these applications of quasi-steady state conditions, however, are difficult to assess because of the following reasons: (1) Aquifers are inherently heterogeneous and flow is always three-dimensional. The number of wells in field experiments is limited and the wells are not fully penetrating the entire thickness of the aquifer as required by Theis solution. As a consequence, few field data have offered convincing evidence of the existence of quasi-steady state conditions. (2) The inverse solution for ill-defined problems (i.e., lack of the necessary conditions, see Mao et al. (2013b) and Yeh et al. (2015a ,b)) always involve uncertainty. (3) The choice of the equivalent homogeneous model (e.g., single-porosity or dual-porosity model) may also have impact on the occurrence of the steady-shape condition (Pedretti et al., 2016). The robustness of application of quasi-steady state conditions to an inverse modeling problem thus is still in question. Here, we focus on the first issue to discuss the validity of steady-shape condition.

In this study, we first offer a quantitative definition of quasi-steady state condition in unbounded homogeneous aquifers. Afterwards, the validity of quasi-steady condition in bounded heterogeneous aquifers is analyzed using the stochastic concept and approach. The temporal evolution of cross-correlations between parameters and the observed drawdown is considered subsequently. At last, a large number of observed drawdown-time curves due to pumping in a field are examined. We then discuss implications of the results and present our conclusions.

2. Quasi-steady state in equivalent homogeneous aquifers

2.1. Two-dimensional, homogeneous aquifers

Based on the equivalent homogeneous conceptual model, a quasi-steady (or steady-state shape) condition can be defined if the temporal changes of hydraulic gradients between all available observation wells are "sufficiently" small. In order to derive a quantitative definition, we will start from the governing equation of two-dimensional flow in homogeneous and isotropic confined aquifer and assume the aquifer is unbounded in all lateral directions. With these assumptions, an analytical solution for the drawdown at a radial distance r from a pumping well was reported by Theis (1935),

$$s(r,t) = \frac{Q}{4\pi T} W(u) \tag{1}$$

where s is the drawdown (initial head minus head at time t), $W(u) = \int_u^\infty \frac{e^{-z}}{z} dz$ is the well function and $u = r^2S/(4Tt)$, S is the storage coefficient, t is time, T is transmissivity, Q is the constant pumping rate.

According to this solution, the hydraulic gradient g along radius direction at (r, t) is:

$$g = -\frac{\partial s}{\partial r} = \frac{Q}{2\pi rT}\exp\left[-\frac{r^2 S}{4Tt}\right] = \frac{Q}{2\pi rT}\exp(-u) \quad (2)$$

At late time (i.e., small u), the gradient g at any location r will asymptotically approach the value of $g_{asym} = Q/(2\pi rT)$, which is independent of time. As u is smaller than 0.01, the relative difference between $g(t)$ and g_{asym} will be less than 1% according to the mathematical properties of the function exp(-u). Under this situation, we can say that a quasi-steady of the cone of depression will exist, if we accept this 1% as the criterion. This situation has been referred to as steady-shape conditions.

Another way to look at this issue is to use the temporal derivative of drawdown (w),

$$w = \frac{\partial s}{\partial t} = \frac{Q}{4\pi Tt}e^{-\left(\frac{r^2 S_s}{4Tt}\right)} = \frac{Q}{4\pi Tt}\exp(-u) \quad (3)$$

Again, at late time (i.e., small u), the temporal change of head (w) at different locations (i.e., different r's) will asymptotically approach the value of $w_{asym} = Q/(4\pi tT)$, which is independent of location r. When u is smaller than 0.01, function exp(-u) will be greater than 0.99, which means that the relative difference of w values at different locations is less than 1%. This is tantamount to stating that head difference between any two different observation locations (a surrogate head gradient) is approximately constant in time with less than 1% relative error. This situation is commonly known as quasi-steady flow condition. As shown above, the quasi-steady condition is equivalent to the steady-shape condition. Note that a quasi-steady state does not imply approximate steady state, where the rate of change in the head is close to zero.

If we assume that the furthest observation well of the two wells is at r_m, in order to ensure all u's at the two locations are less than 0.01, t should be greater than $100{r_m}^2 S/4T$, which is regarded as the time to reach quasi-steady condition (i.e., onset or kickoff time) for area $r\in(0, r_m]$ in the two-dimensional, unbounded, homogeneous aquifer. At this time, the water supplying rate (released water per unit time, with the same dimension as Q) from area $r\in(0, r_m]$ is:

$$2\pi\int_0^{r_m} Sw(r,t)rdr = Q\left[1-\exp\left(-\frac{{r_m}^2 S}{4Tt}\right)\right] \quad (4)$$

According to Eq. (4), in order to reach an approximate quasi-steady with less than 1% error, 99% of the pumped water must come from outside of the radius r_m. In this situation, the shape of the cone of depression for area $r\in(0, r_m]$ does not change significantly and the quasi-steady of the depression approximately exist. As illustrated in Fig. 1(a), although drawdown s increases logarithmically with t and never attains steady state, the head gradient can be approximately regarded as solely a function of r within a circular quasi-steady state region, and the area of region ($\propto r^2$) expands linearly with t. That is, the drawdown-log time lines at different r values will be parallel as illustrated in Fig. 1(a). This is the theoretical definition of the quasi-steady in a two-dimensional, homogeneous aquifer during a pumping test.

Next, we will examine the effects of three-dimensional flow on the definition of quasi-steady conditions. Notice that we have defined the quasi-steady state condition using either spatial or temporal derivatives of drawdown as a criterion. In the next section as well as the rest of this paper, we choose the temporal derivative of drawdown (w) as the criterion, rather than the spatial derivative or spatial gradient (g), although the latter is a more intuitive concept. Several reasons for this choice are: first, the spatial gradient (g) at a location cannot be accurately obtained since observation wells are often sparsely spaced. Second, to examine the quasi-steady, N drawdown-time curves usually require to calculate (N-1)N/2 pairs of head differences (see (Bohling et al., 2002)). To the contrary, only time derivatives of these drawdowns are needed if time derivative of drawdown concept (w) is adopted.

2.2. Three-Dimensional, homogeneous aquifers

Consider the flow induced by pumping from a well in a homogeneous, three-dimensional aquifer with infinite thickness and without any boundary in other directions. The analytical solution of drawdown caused by continuous pumping at a point (i.e., point sink) is,

$$s(r,t) = \frac{Q}{4\pi rK}erfc\left(\sqrt{u}\right) \quad (5)$$

where S_s is the specific storage, K is the hydraulic conductivity, $\mathrm{erfc}(u) = \frac{2}{\sqrt{\pi}}\int_u^\infty e^{-z^2}dz$ is the complementary error function, and $u = r^2 S_s/(4Kt)$. According to this solution, the three-dimensional drawdown at any location will asymptotically reach a value of $s_{asym} = Q/(4\pi rK)$ when t is very large (Fig. 1(c)). This result is similar the theoretical drawdown behavior during pumping in a two-dimensional leaky aquifer system, in which the drawdown also tends to stabilize in a log time-drawdown plot (Renard et al., 2009). That is, the rate of change of drawdown will approach zero or the flow is close to steady state, where the change in storage approaches zero. In contrast, drawdown, based on Theis solution for non-leaky aquifer, increases with time without a finite bound (Fig. 1(a)).

We then define an approximately steady-state condition as the situation where the relative difference between drawdown $s(r, t)$ and s_{asym} less than 1%. For this approximate steady state flow condition, the function $\mathrm{erfc}(\sqrt{u})$ should be greater than 0.99, which requires that $\sqrt{u}$ is smaller than 0.01. If we assume that the furthest observation well is at r_m, then t should be greater than $(100)^2 r_m^2 S_s/4K$ such that the approximate steady state exists.

Next, we examine the time to reach quasi-steady or steady shape condition. For three-dimensional flow to a well, the temporal derivative of drawdown (w) is,

$$w(r,t) = \frac{Q\sqrt{S_s}}{8(\pi tK)^{3/2}}\exp(-u) \quad (6)$$

Eq. (6) shows that similar to the two-dimensional case, the exp(-u) will asymptotically reach 1.0 at late time for different r's such that the quasi-steady exists. In order to reach the quasi-steady condition in a three-dimensional flow, t should be greater than $100{r_m}^2 S_s/4K$ to satisfy the 1% tolerance according to the previous discussion. That is, the time to reach an approximate steady-state in the three-dimensional converging flow induced by pumping is 100 times larger than the time to the quasi-steady (Fig. 1(c and d)).

In summary, we here provide consistent definitions for approximate steady state and quasi-steady state (or steady shape) conditions for two- and three-dimensional flow in unbounded, homogeneous aquifers. It is noteworthy that since S/T equals S_s/K, there is no difference in time to satisfy the quasi-steady condition with regard to two- and three-dimensional flows in the same homogeneous aquifer. In the next section, we will investigate the effects of heterogeneity on these definitions.

3. Quasi-steady state in heterogeneous aquifers

3.1. Stochastic analysis

(1) First order approximation

In order to address the effect of heterogeneity, we will represent spatial variability of $\ln K$ and $\ln S_s$ at in a field as two mutually

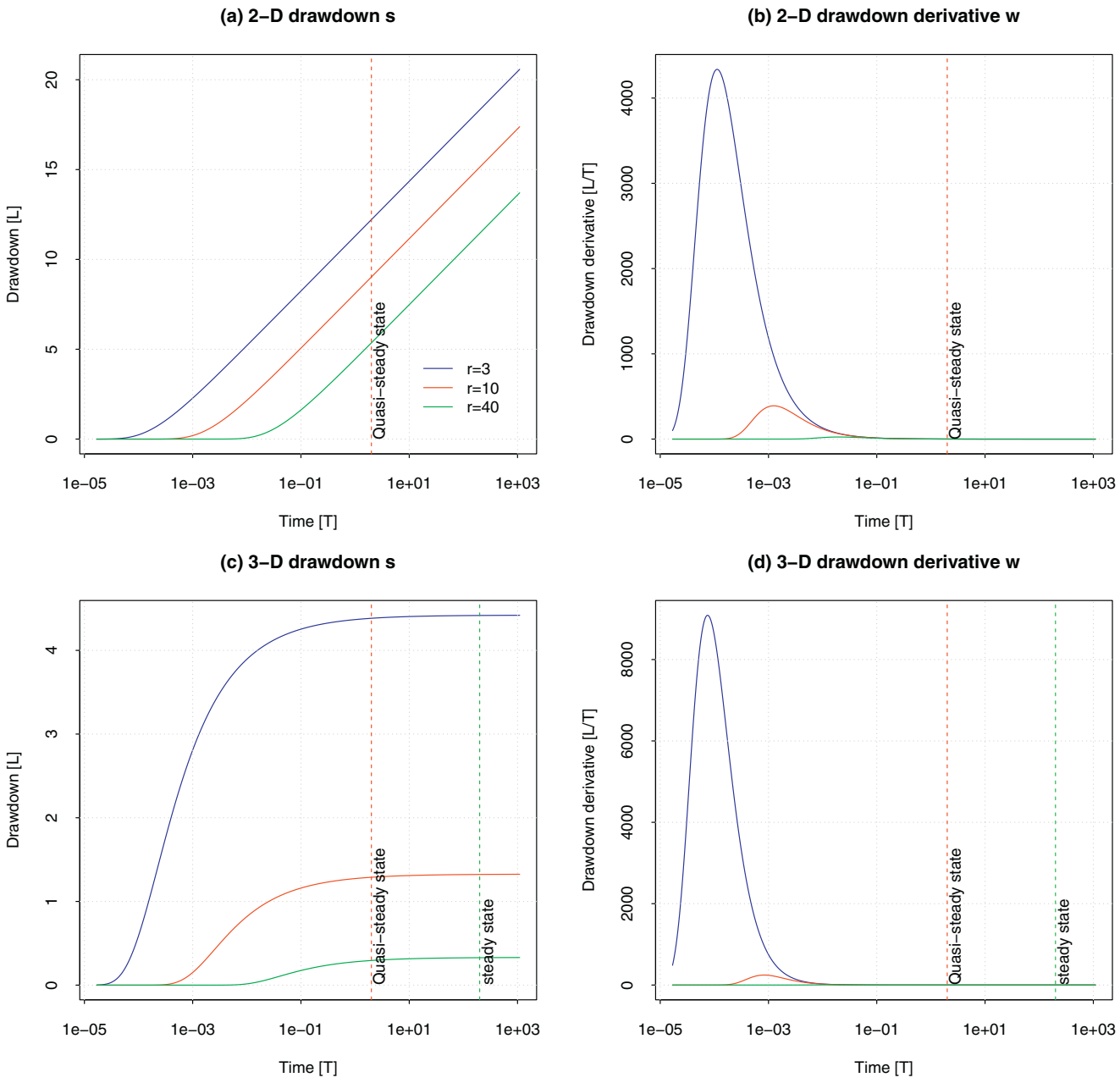

Fig. 1. The drawdown (s) and temporal derivatives of drawdown (w) at different locations ($r = 3$, 10, and 40) in (a, b) 2-D and (c, d) 3-D aquifers. The red and green dot lines denote the time reaching steady shape and steady state according to their definitions ($r_m = 40$). Parameter $K = 0.2$ [L/T], $S_s = 1.0 \times 10^{-5}$ [L^{-1}], thickness $U = 30$ [L], constant pumping rate $Q = 100$ [L^3/T]. (For interpretation of the references to colour in this figure legend, the reader is referred to the web version of this article.)

independent random fields, which are characterized by their own joint probability distributions. We further assume that the means and covariances are sufficient for depicting the distributions (i.e., multi-Gaussian distributions). The covariance is described by the exponential function with a variance and correlation scales in the three dimensions. The natural logarithms of K ($\ln K$) and S_s ($\ln S_s$) are expressed as $\ln K = F + f$ and $\ln S_s = P + p$, respectively. F and P are their means and f and p are their perturbations. Likewise, the output state variable v (drawdown s or its temporal derivative w) can also be expressed as the summations of means (V) and perturbations (ξ). Since the analysis will be carried out numerically, the parameter fields f and p are discretized into two $N \times 1$ vector $\mathbf{f} = [f_1, f_2, \ldots, f_N]^{\mathrm{T}}$ and $\mathbf{p} = [p_1, p_2, \ldots, p_N]^{\mathrm{T}}$, where N is the number of elements in the numerical model and superscript T denotes transpose. Let us denote $\aleph$ as an forward operator mapping hydraulic parameters to observation v at location $\mathbf{x}_i$ and time t (through numerical model). Based on first-order analysis (Sun et al., 2013), we have,

$$\begin{aligned} v(\mathbf{x}_i, t) &= V(\mathbf{x}_i, t) + \xi(\mathbf{x}_i, t) = \aleph(\mathbf{F} + \mathbf{f}, \mathbf{P} + \mathbf{p}) \\ &\approx \aleph(\mathbf{F}, \mathbf{P}) + \left(\frac{\partial \aleph}{\partial \mathbf{f}}\bigg|_{\mathbf{F},\mathbf{P}} \right)^T \cdot \mathbf{f} + \left(\frac{\partial \aleph}{\partial \mathbf{p}}\bigg|_{\mathbf{F},\mathbf{P}} \right)^T \cdot \mathbf{p} \end{aligned} \tag{7}$$

Taking expectation (with angle brackets) on both sides of the equation, we obtain that,

$$\begin{aligned} &\langle V(\mathbf{x}_i, t) + \xi(\mathbf{x}_i, t) \rangle = V(\mathbf{x}_i, t) \\ &\approx \left\langle \aleph(\mathbf{F}, \mathbf{P}) + \left(\frac{\partial \aleph}{\partial \mathbf{f}}\bigg|_{\mathbf{F},\mathbf{P}} \right)^T \cdot \mathbf{f} + \left(\frac{\partial \aleph}{\partial \mathbf{p}}\bigg|_{\mathbf{F},\mathbf{P}} \right)^T \cdot \mathbf{p} \right\rangle \\ &= \aleph(\mathbf{F}, \mathbf{P}) \end{aligned} \tag{8}$$

This equation indicates that the mean heads **V** are approximated by the governing equation with the mean values of the parameters **F** and **P**. Accordingly, the perturbation of output state variable (ξ) due to heterogeneity can be calculated as,

$$\xi(\mathbf{x}_i,t) \approx \left(\left.\frac{\partial \aleph}{\partial \mathbf{f}}\right|_{\mathbf{F},\mathbf{P}}\right)^T \cdot \mathbf{f} + \left(\left.\frac{\partial \aleph}{\partial \mathbf{p}}\right|_{\mathbf{F},\mathbf{P}}\right)^T \cdot \mathbf{p}$$
$$\approx \sum_{k=1}^{N}\left[\left.\frac{\partial \xi(\mathbf{x}_i,t)}{\partial f_k}\right|_{\mathbf{F},\mathbf{P}} f_k + \left.\frac{\partial \xi(\mathbf{x}_i,t)}{\partial p_k}\right|_{\mathbf{F},\mathbf{P}} p_k\right] \quad (9)$$

where f_k and p_k are perturbations of ln$K$ and lnS_s at location $\mathbf{x}_k$ ($k=1, 2, \ldots, N$), respectively. This equation indicates that the perturbation of observation ξ at location $\mathbf{x}_i$ and time t is a weighted sum of f_k and p_k at all the locations, which represent the parameter variability or uncertainty. The weights are the corresponding sensitivity values evaluated at the mean parameter fields **F** and **P**. Multiplying Eq. (9) by itself and taking expectation on both sides, we obtain the variance of ξ as,

$$\sigma_\xi^2 = \sum_{i=1}^{N}\sum_{j=1}^{N}\frac{\partial \xi}{\partial f_i}C_{ij}\frac{\partial \xi}{\partial f_j} + \sum_{i=1}^{N}\sum_{j=1}^{N}\frac{\partial \xi}{\partial p_i}D_{ij}\frac{\partial \xi}{\partial p_j} \quad (10)$$

where C_{ij} and D_{ij} are elements of the covariance matrices of ln$K$ and lnS_s, which are calculated based on assumed variance, correlation scales, covariance functions and the three-dimensional coordinates of $\mathbf{x}_i$ and $\mathbf{x}_j$.

(2) Numerical implementation

According to the first-order analysis, Eq. (8), the mean heads, **V**, are approximated by the governing equation with mean values of parameters **F** and **P**, which are assumed to be spatially invariant. Thus, we calculate the mean heads, induced by a constant-rate pumping, in a three-dimensional, homogeneous and isotropic confined aquifer, using the following groundwater flow equations:

$$S_s\frac{\partial h}{\partial t} = \nabla\cdot(K\nabla h) + Q_p\delta(\mathbf{x}-\mathbf{x}_p)H(t-t_0) \quad (11)$$

subjected to boundary conditions and initial conditions,

$$h|_{\Gamma_1} = h_0,\ -\mathbf{q}\cdot\mathbf{n}|_{\Gamma_2} = q_0 \quad (12)$$

$$h|_{t=0} = h_{\text{ini}} \quad (13)$$

Again, K and S_s are their mean values in Eq. (11). Pumping is at location $\mathbf{x}_p$ starting from t_0, H is the Heaviside step function, and δ is the Dirac delta function. $\mathbf{q}$ is the Darcian flux, h_0 is the prescribed total head at the Dirichlet boundary Γ_1, and q_0 is the specified flux at the Neumann boundary Γ_2, and $\mathbf{n}$ is the unit vector normal to the boundary Γ_2, h_{ini} is the initial head distribution.

Taking derivative of Eqs. (11)–(13) with respect to t leads to the governing equation of the temporal derivative of the mean drawdown (w):

$$S_s\frac{\partial w}{\partial t} = \nabla\cdot(K\nabla w) + Q_p\delta(\mathbf{x}-\mathbf{x}_p)\delta(t-t_0) \quad (14)$$

subjected to boundary conditions and initial conditions,

$$w|_{\Gamma_1} = 0,\ -K\nabla w\cdot\mathbf{n}|_{\Gamma_2} = 0 \quad (15)$$

$$w|_{t=0} = 0 \quad (16)$$

Note that w is described by the same equation as in Eq. (11), except that the constant pumping rate now becomes an instant impulse. Again, K and S_s are their mean values.

The simulations are performed using a finite element code VSAFT3 (Variably Saturated Flow and Transport in 3-D) developed by Srivastava and Yeh (1992). This code is able to simulate variably saturated flow and transport problems and perform sensitivity/cross-correlation analysis. Its robustness has been widely tested against different flow and transport problems during the last two decades (Berg and Illman, 2011; Zha et al., 2015). Based on Eq. (8), we solve Eqs. (11)–(13) and Eqs. (14)–(16) to approximate the mean h and w behaviors using VSAFT3 with **F** and **P** (or mean values of K and S_s) for each element.

To evaluate the variance of observation v using Eq. (10), the sensitivities ($\partial\xi/\partial f_i$ and $\partial\xi/\partial p_i$, for $i=1, 2, \ldots, N$) have to be known. We use adjoint method to calculate sensitivities due to its high efficiency in this problem with one observation and N parameters (Zhu and Yeh, 2005). Perturbation method needs running VSAFT3 ($N+1$) times (N for perturbed parameters at different locations and one for mean flow equation) while adjoint method only requires $1+1$ times (one for adjoint equation and one for mean flow equation).

Since the governing equations of w and h only differ in the source terms, these two variables share the same adjoint variable and adjoint state equation (Zhu and Yeh, 2005):

$$-S_s\frac{\partial \varphi}{\partial t} = \nabla\cdot(K\nabla\varphi) + \delta(\mathbf{x}-\mathbf{x}_{obs})\delta(t-t_{obs}) \quad (17)$$

subjected to the boundary conditions and initial conditions:

$$\varphi|_{\Gamma_1} = 0, K\nabla\varphi\cdot\mathbf{n}|_{\Gamma_2} = 0 \quad (18)$$

$$\varphi|_{t=0} = 0 \quad (19)$$

Again, the adjoint equation is solved using VSAFT3 using the same mean parameters assigning to every element. The sensitivities for the observation ξ at location $\mathbf{x}_{\text{obs}}$ and time t_{obs} with respect to parameters at location $\mathbf{x}_k$ ($k=1, 2, \ldots, N$) are then obtained via integration (Leven and Dietrich, 2006; Lu and Vesselinov, 2015):

$$\frac{\partial \xi(\mathbf{x}_{obs},t_{obs})}{\partial f(\mathbf{x}_k)} = -\int_{\Psi}\int_{\Omega_k}\frac{\partial K(\mathbf{x})}{\partial f(\mathbf{x}_k)}(\nabla\varphi(\mathbf{x},t_{obs}-t))^{\mathrm{T}}\cdot\nabla V(\mathbf{x},t)\mathrm{d}\Omega\mathrm{d}t \quad (20)$$

$$\frac{\partial \xi(\mathbf{x}_{obs},t_{obs})}{\partial p(\mathbf{x}_k)} = -\int_{\Psi}\int_{\Omega_k}\frac{\partial S_s(\mathbf{x})}{\partial p(\mathbf{x}_k)}\varphi(\mathbf{x},t_{obs}-t)\frac{\partial V(\mathbf{x},t)}{\partial t}\mathrm{d}\Omega\mathrm{d}t \quad (21)$$

where $\Psi\in[0, t_{\text{obs}}]$ is the integration time interval, and Ω_k is the domain of element containing $\mathbf{x}_k$. The mean state variable V is solved from Eqs. (11)–(13) for variable h and from Eqs. (14)–(16) for variable w with input of mean parameters F and P. The sensitivity of the variable considered at an observation port at every time step is necessary for the following analysis. The adjoint models are, however, solved only once for the latest observation time. Then, the adjoint variables of the same observation port at other time steps are merely a temporal shift of the latest one (Lu and Vesselinov, 2015; Zha et al., 2016) due to the linear nature of adjoint models (Eqs. (17)–(19)) in terms of time.

The numerical evaluation of Eqs. (20) and (21), which requires little computational cost and coding, has also been implemented in VSAFT3. The integration over time is only summation over all time steps. The spatial gradients or temporal gradients are approximated by shape function or finite difference in the numerical model.

Note that first-order approximation is built upon small perturbation theory. It may yield inaccurate mean and variance of the state variable if the parameter variance is large. Nevertheless, a vast number of applications (Dagan, 1982; Zhang and Yeh, 1997) report that the first-order approximation is a practical tool since it yields satisfactory results with least computational cost as long as the heterogeneity is not extremely high. In contrast, while Monte Carlo simulation is free of this assumption, it requires a large number of realizations to yield accurate results, which makes Monte Carlo simulations of a 3-D transient flow unfordable.

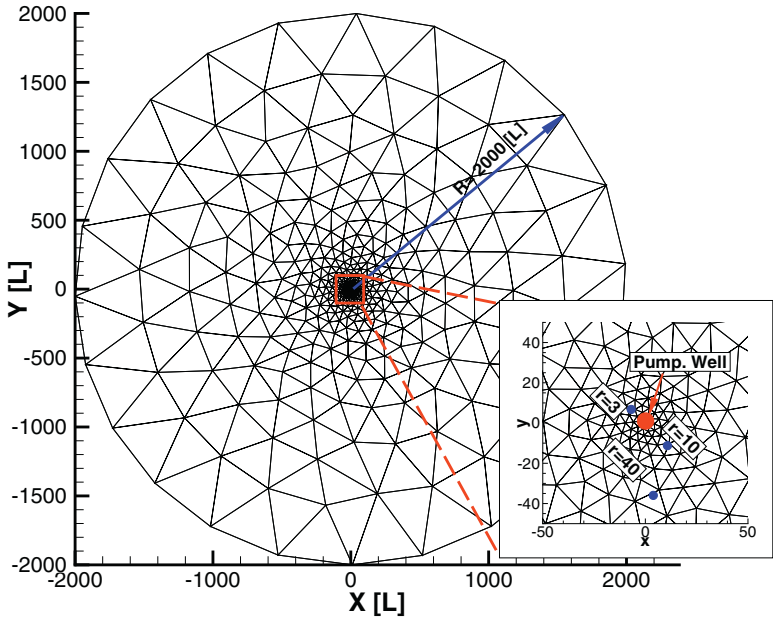

Fig. 2. Horizontal mesh for the numerical model. The radius of the cylinder is $R = 1000$ [L]. The average mesh size is 1 [L] for the pumping location at the center of the domain, and the mesh size increase gradually to 400 [L] at the boundary.

3.2. Numerical experiments

To conduct the stochastic analysis, a 3-D cylinder-shaped synthetic aquifer surrounded by no-flux boundary (unless noted otherwise) is designed (Fig. 2). The radius and height of the cylinder are $R = 2000$ [L] and $U = 30$ [L]. The mean K and S_s values are 0.2 [L/T] and 1.0×10^{-5} [L^{-1}], respectively: they are any units which are consistent with K. The pumping well is located at the domain center with a constant pumping rate of 100 [L^3/T]. Drawdowns from three observation wells, located at 3, 10 and 40 away from the pumping well, are collected during pumping. Different combinations of the variances, and correlation scales of the parameters are used to demonstrate their influences. The influences of numerical model settings and well screen interval are also considered. The numerical model discretizes the numerical domain into triangular prisms. To save computational time, the average mesh size is 1 [L] for the pumping location at the center of the domain, and the mesh size increase gradually to 400 [L] at the boundary. In the vertical direction, 30 layers with a uniform thickness of 1 are used. The total numbers of elements and nodes are 25,470 and 13,547. It should be noted that this type of discretization is compatible with the converging flow nature of pumping (Schneider and Attinger, 2008; Zech and Attinger, 2015). Based on this synthetic aquifer, the effects of boundary conditions, well-screen length, K_s and S_s heterogeneity are investigated and discussed below.

3.2.1. Influence of the numerical settings

Before conducting stochastic analysis, the influences of numerical settings (i.e., domain size, boundary condition, and discretization) on the stochastic analysis are examined. Fig. 3(a) illustrates the mean drawdown-time curves at a fully-screened observation well due to pumping in a fully penetrating well in aquifers with constant head and no-flux boundary conditions. These mean curves are simulated with the three-dimensional governing flow equations using the mean K_s and S_s. It indicates that the drawdowns at the two observation locations at a distance of 10 and 40 start to noticeably experience the boundary conditions (i.e., no flux, constant head, and unbounded conditions) at $t = 40$ [T]. On the other hand, the aquifer will reach quasi-steady conditions for $r_m = 40$ [L] approximately at $t \approx r_m^2 S_s/(4K) = 2$ [T], which is calculated using the mean properties of the aquifer. That is, the time for drawdown to encounter boundary is 20 times of the time to reach the quasi-steady state conditions. A smaller domain will reduce the time to the boundary. According to Fig. 3(a), it is found that the time to feel boundary (t^*) is proportional to area of the domain (i.e., $t^* \propto R^2$), which is reasonable according to Theis solution. In spite of the drawdown's travel time to the boundary, once it reaches the boundary, the flow field will deviate from the quasi-steady state conditions. It can become a steady state flow if the boundary is constant head, or another transient flow conditions if the boundary is impermeable. Note that boundaries are can be regarded as the heterogeneity at outer space with great contrasts in comparison with the hydraulic properties inside the simulation domain. Nevertheless, such information may provide useful information about the boundary (i.e., significant heterogeneity at far-field). This fact was demonstrated by Sun et al. (2013), who showed that late time drawdown data from HT survey can detect the location of the impermeable boundary.

In order to minimize the simulation cost without aggravating the accuracy, we test the influence of vertical discretization on the result accuracy. The horizontal mesh is fine enough at the location where the hydraulic gradient is high. Again, both pumping and observation wells are fully screened. Numerical test shows that the vertical discretization has little impact on the calculated mean drawdown. However, as indicated in Fig. 3(b), the calculated variance (using Eq. (10) with variance of $f = 1$, correlation scales of Domenico and Schwartz (1998), Domenico and Schwartz (1998) and Berg and Illman (2011)^T, and variance of $p = 0$) is significantly influenced by the vertical mesh size Δz. The larger the Δz, the larger the calculated variance. Based on Eq. (10), we infer that this difference is due to the discretization error in the covariance function of K and S_s since the mean drawdown and the sensitivity result are not influenced by Δz. The numerical model artificially increases the covariance C and D (see Eq. (10)) if the vertical discretization is not fine enough (compared to the vertical correlation scale) and thus it increases the calculated variance. In the following cases, we make sure that Δz is less than the 1/3 of the vertical correlation scale in order to minimize this impact.

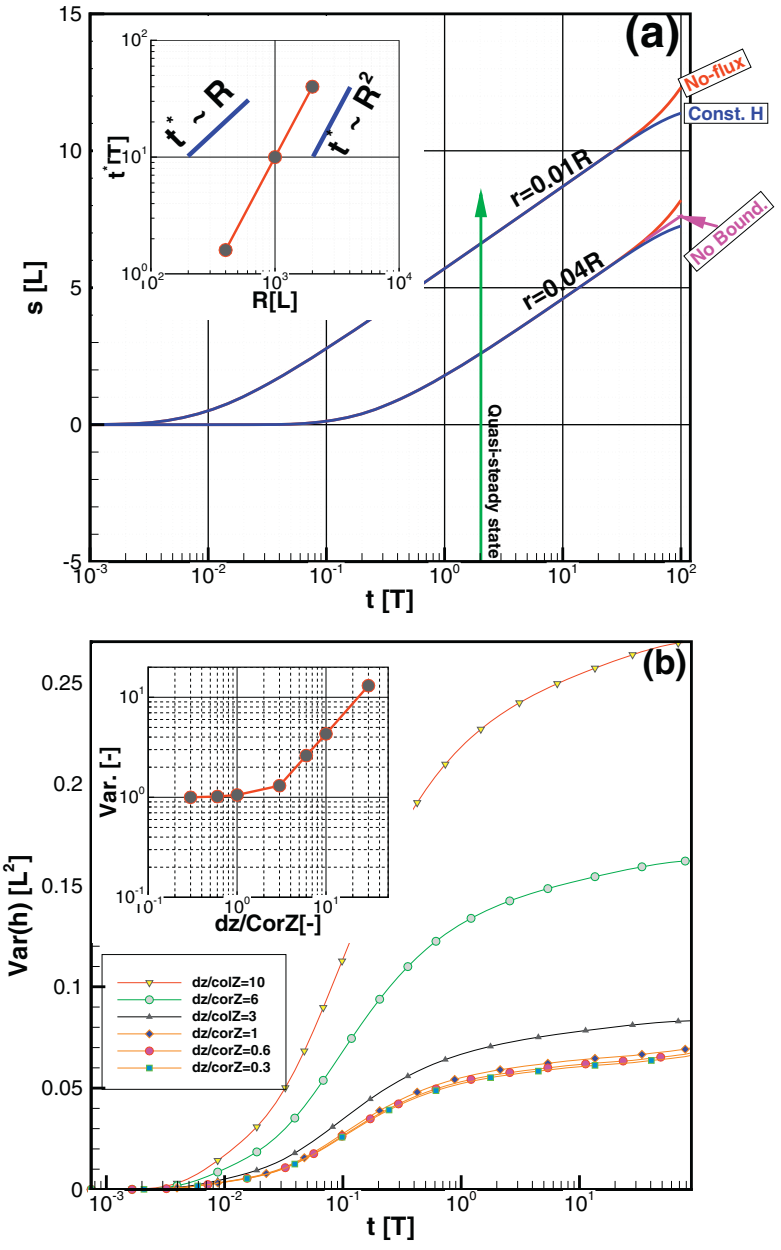

Fig. 3. Effects of model settings on the analysis. (a) The influence of boundary conditions on drawdown at late time and the relationship between domain size R and the time t^* to feel the boundary. (b) The calculated variance values versus time based on different vertical discretization schemes. The relationship between the calculated head variance and the dz/CorZ (ratio of vertical mesh size to the vertical correlation scale of ln$K$).

3.2.2. Influences of the well screen interval

An observation well with a long screen length generally observes the averaged head over a great volume of the aquifer around the well. On the other hand, a pumping well with a long screen length may distribute excitation over a greater volume. In other words, the screen lengths of either pumping well or observation well may affect the time to ergodicity and in turn, quasi-steady state conditions. Results of our numerical investigations of the impact of well screen length on mean drawdown behavior are presented in Fig. 4(a) as cases 1, 2, 3, and 4 (indicated by the pink, green, black and orange lines, respectively). Case 1 denotes the situation where short screen lengths (0.1 U) are used for both observation well and pumping well. Case 2 represents the case where pumping well and observation well are fully screened (U) over the depth of the aquifer, and lastly, fully screened pumping well but shortly screened observation well are considered in case 3, and partially screened pumping well but fully screened observation well are considered in case 4. This figure also displays the drawdown observed at different radial distances (i.e., $r=3$, $r=10$, and $r=40$).

As shown in this figure, for $r=3$, the drawdown in case 1 acts as 3-D flow first and then behaves like a 2-D flow (i.e., drawdown grows linearly with logrithm of time). It then starts to feel the boundary at large time. The magnitude of drawdown in case 1 is larger than those in cases 2, 3, and 4 at $r=3$. Such differences become smaller at $r=10$ and are negligible for $r=40$. Notice those drawdowns in cases 2, 3, and 4 are almost identical, in spite of the distance from the pumping well. They all behave in a manner similar to the drawdown-time curves in 2-D aquifers. These results are somewhat expected since the aquifer is homogeneous (using the mean parameters) and the differences lie in the evolution of the flow field.

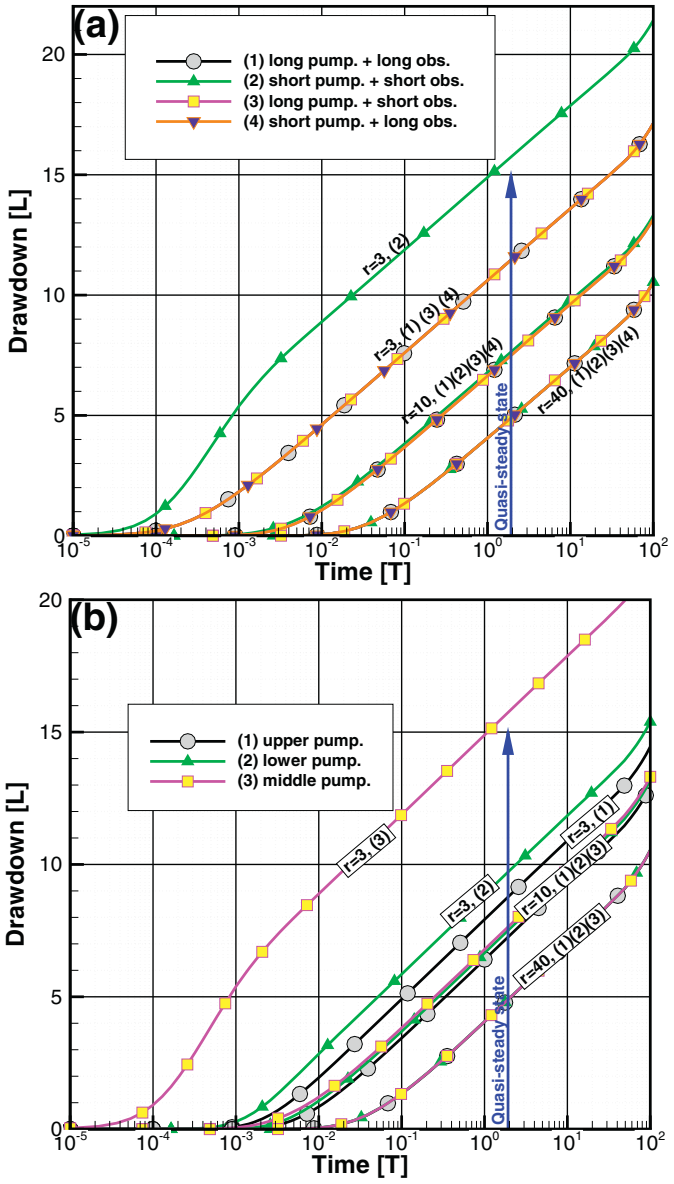

Fig. 4. The influence of (a) well screen lengths and (b) pumping screen locations on the temporal evolution of the drawdown values. In (b) the observation well is assumed to have short screen length located at the middle of the domain vertically. (For interpretation of the references to colour in this figure legend, the reader is referred to the web version of this article.)

The influences of the pumping interval locations are displayed in Fig. 4(b). The observation well screen length is 0.1 U and is located at the middle part of the domain. The short-screened pumping well is located at the upper (case 1), middle (case 2) or lower (case 3) part of the domain. The magnitude of drawdown in case 3 is larger than those in cases 1 and 2 at $r=3$. The reason is that the 3-D distance between pumping and observation wells in case 3 is smaller than those in other cases. Again, such differences become smaller at $r=10$ and are negligible for $r=40$. Overall, Fig. 4 indicates that the onset time of the quasi-steady is not influenced by the screen length and its location.

3.2.3. *Effects of heterogeneity of* k

Fig. 5(a) and (b) show the temporal evolution of the mean head and mean w (temporal head derivative) as well as their upper and lower bounds at the observation well ($r=10$ and 40) in the aquifer with the variability of ln$K$. Variance of f (i.e., perturbation of ln$K$) of the aquifer is assumed to be 1, and correlation scales are 10 in horizontal direction and 3 in vertical directions, respectively. Variance of lnS_s is assumed to be zero. Based on these geostatistical parameters, we then construct the covariance C_{ij} and calculated head variance based on Eq. (10).

These upper and lower bounds are calculated by adding or subtracting one standard deviation of the corresponding state variables, based on the calculated variance using the first-order analysis (i.e., Eq. (10)). Fig. 5(a) shows that the mean drawdown values continuously increase at the two locations ($r=10$ and 40), but the mean head gradient stabilizes at $t>2$, reaching quasi-steady at time equal to $r_m{}^2S_s/(4K)$, where the parameters are their mean values. The quasi-steady then is interrupted by the boundary after $t>40$. If we examine the upper and lower bounds of the head at steady state, we find that they also continuously increase and reach some constant values but the gap between the upper and the lower bounds are large (i.e., large variability in head at late time).

At the same time, the mean temporal derivatives of heads at the given observation locations first increase to the peak values and then decrease gradually (Fig. 5(b)). Moreover, the temporal derivatives of mean heads at different locations ($r=10$ and $r=40$) approach the same value approximately at $t>2$ (see solid red and blue lines in Fig. 5(b)). These behaviors are similar to those in unbounded homogeneous aquifers, and the time $t=2$ (Fig. 3(a)) can be regarded as the minimum time to synchronize all the head temporal change (w) at different locations ($r_m=40$), i.e., steady-shape conditions, if only mean head is considered. However, the variability of w does not fade away after the mean flow reaches quasi-steady as indicated by the bounds of w in Fig. 5(b). This means that due to the variability of K, there are many possible values of w at $t>2$ at different locations, even the mean values of w at different locations have synchronized (drawdowns decrease at the same rate). In other words, the onset time of quasi-steady state is only true for mean head, and is delayed and different in single realization due to the heterogeneity of K.

Fig. 6(a) presents another look at the effects of the heterogeneity of K on the development of quasi-steady state. The green line in the figure represent the relative differences of drawdown rate w values (i.e., 1-exp(-u), where $u=r_m{}^2S/(4Tt)$, see the definition of quasi-steady state above) at different locations in the area $r\in(0, r_m]$ based on homogeneity assumption. As discussed before, heterogeneity introduces additional variability of w. The coefficient of variation C_w, defined by standard deviation of w normalized by w, is plotted as a function of time in Fig. 6. If the threshold of 1% error (red solid line, the relative difference between w values in the area $r\in(0, r_m]$) is chosen, both the deviation of mean flow and the C_w should be less than 1% to reach the quasi-steady condition. For the case with a variance of 0.1 and correlation scale of 10 and 3 in horizontal and vertical directions, the kickoff time of quasi-steady flow is $t=1.1$, which is less than the time ($t=2$) to reach the quasi-steady state for the mean flow. However, if the correlation scales are larger (e.g., 20 and 6 in horizontal and vertical directions, respectively), the coefficient of variation of w increases and the kickoff time is postponed to 3.1, which is only slightly later than that in the homogeneous case. If we keep the correlations but increase the variance to 1.0, the kickoff time is further delayed to $t=8.9$, which is much larger than $t=2.0$ in the mean flow. Again, heterogeneity affects the time required to reach a quasi-steady state flow situation.

This implies that a larger variance or larger correlation scales of K will lead to a slowly decaying variability of w. Fig. 6(a) also gives relationship between the change of the variance or correlation scales versus the change of time when C_w is less than 1% (t^*). As indicated in Fig. 6(a), t^* increases by 8 times or 36 times while the variance or the correlation scales of f increases by 10 times,

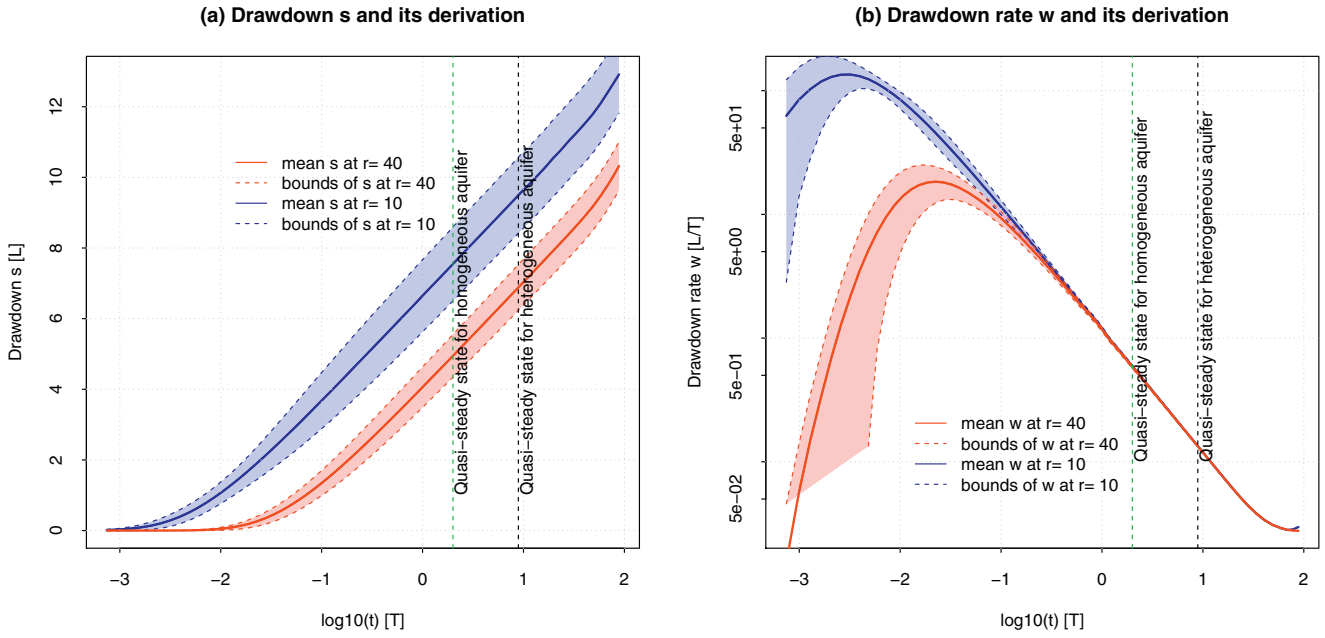

Fig. 5. The temporal evolutions of drawdown s and its derivative w at different observation locations ($r = 10$ or 40). The shadow area indicating the bounds is calculated by adding or subtracting standard derivation. Variance of $f = 1$, correlation scales are 10, 10, and 3. Variance of $p = 0$. (For interpretation of the references to colour in this figure legend, the reader is referred to the web version of this article.)

respectively. Their relationships can be analyzed based on Eq. (10). Since variance of f is a linear factor in Eq. (10), it is expected that C_w is proportional to the square root of the f variance. The change of time t^* is determined by the f variance and the slope of the C_w versus t curve. In contrast, the correlation scales are nonlinear factors in Eq. (10) and t^* increases rapidly with the increase of correlation scales in three dimensions. However, it is expected that the increase will slow down and vanish as the correlation scales approach the dimensions of the domain.

It should be noted that after $t > 40$, the flow is influenced by the boundary condition. Thus, the quasi-steady in each realization of the ensemble may not exist until the flow until steady state is reached if there is recharge boundary, although it exists on the average sense (i.e., the mean head). On the other hand, if the boundary is impermeable, the quasi-steady state will not exist either in the mean flow nor the observed head.

These findings are consistent with the fact that during the expansion of the cone of depression, the head or head gradient will be influenced by the heterogeneity within the depression (see Sun et al. (2013)) as time progresses. The smaller variance or the smaller correlation scale is, the less correlated and more independent the heterogeneity within the cone is. As a result, the head difference at different parts of the cone can easily equalize, ergodicity for the equivalent homogeneous model can be met, and an approximate quasi-steady can likely occur. On the other hand, under large variance and correlation scales conditions, the flow will likely take a longer time to sample all heterogeneity such that head gradient takes a longer time to stabilize, and ergodicity will not be met, as explained in Yeh et al. (2015a).

3.2.4. Effects of heterogeneity of S_s

A large number of previous works have investigated only the influences of K on quasi-steady regime, without studying effects of variability of S_s. Here, Fig. 7(a) and (b) show the drawdown and drawdown rate as a function of time, respectively, due to the variability of S_s (variance of $p = 1$, correlation scales are 10, 10, and 3) only. According to the figure, the variability of flow field due to the variability of S_s is smaller than that due to variability of K with the same variance and correlation scales (Fig. 7 versus Fig. 5), corroborating other studies (Mao et al., 2013a; Sun et al., 2013). The variability of S_s is small after the mean flow reaches quasi-steady, but it increases when the flow is influenced by the boundary.

Again, another way to examine the influence of S_s heterogeneity on the development of quasi-steady is shown in Fig. 6(b). We find that all drawdowns at $t > 5.2$ satisfy the 1% threshold when variance of $p = 1$, and correlation scales are 10, 10 and 3, but they fail to maintain the situation when $t > 40$ due to boundary effects. When the variance decreases to 0.1, the heterogeneity of $\ln S_s$ does not influence the time to reach quasi-steady. The increase of horizontal correlation scales from 10 to 20 significantly delays the time to quasi-steady conditions. As indicated in Fig. 6(b), t^* increases by 4 times or 40 times while the variance or the correlation scales of p increases by 10 times, respectively.

The above results indicate that if the domain is sufficiently large (determined by R), the quasi-steady regime exists in the mean drawdown of the equivalent homogenous aquifer. At early time, three-dimensional flow does not have significant impact on the drawdown-time curve, but the heterogeneity of K and S_s will influence the head distributions at different time, and will delay the time to reach quasi-steady conditions. In other words, a longer time of pumping is needed to develop quasi-steady regimes in heterogeneous aquifer. However, a longer pumping time also increases the probability of encountering boundaries or large-scale heterogeneity with great contrasts, which corrupts the established quasi-steady state conditions.

3.2.5. Heterogeneity and well screen length

The standard deviations of s and w due to the heterogeneity of K based on different screen intervals of wells are shown in Fig. 8(a) and (b), respectively. The variance of $\ln K$ is 1, and correlation scales are 10, 10 in horizontal directions and 3 in the vertical direction. Fig. 8(a) shows that the case in which both pumping well and observation well with a short screen length has the largest variability in drawdown observations when $r = 10$. In contrast, the case in which both wells using a long screen length has the smallest variability in s. The cases where one of the wells (either the

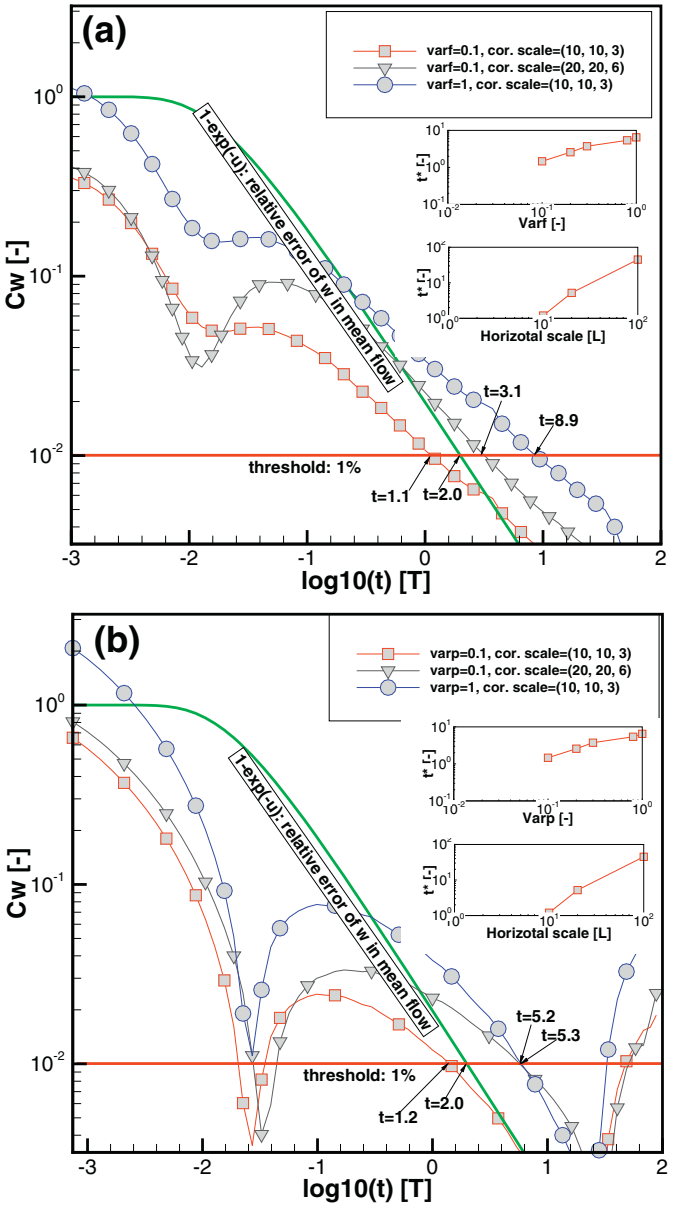

Fig. 6. Coefficient of variation C_w (defined by standard deviation of w normalized by w) versus time introduced by heterogeneity of (a) f or (b) p. The green line is 1-exp(-u) indicating the relative error of w in the mean flow according to Eq. (3). C_w should also be less than 1% based on the definition of steady shape condition in heterogeneous aquifer. The relationships between correlation scales or variances of f and p and the kickoff time t^* (when $C_w < 1\%$) are also displayed. (For interpretation of the references to colour in this figure legend, the reader is referred to the web version of this article.)

pumping well or observation well) is equipped with a short well screen and the other with long well screen, result in the same drawdown standard devations. Their values are slightly larger than that of the case where both pumping well and observation well are equipped with a long well screen. On the other hand, they are smaller than that of the case where both pumping well and observation well are equiped with a short well screen.

These differences are negligible when $r = 40$. Similar differences can be observed in Fig. 8(b) where the standard deviation of drawdown rate is plot as a function of time. The notable differences are now only restricted to very early time. This indicates that the length of the well screens has little impact on the quasi-steady state conditions when the heterogeneity is presented.

These results are consistent with ergodicity concept embedded in stochastic subsurface hydrolgy as explained in Yeh et al. (2015a, b). That is, the flow process has to sample enough heterogeneity such that its behavior is representative (or ergodic), reflecting effects of all heterogeneity. This ergodicity can be met either by pumping for a long period of time or artifically using long well screens for pumping or observation wells. The excitation from at a point sink takes time to encounter heterogeneity at different parts of the aquifer. As pumping lasts a long period of time, the head at an observation point then experiences sufficient heterogeneity and reaches ergodicity. On the other hand, a fully-screened observation well, itself, has imposed spatial averaging process, which averages the heterogeneity experienced over the screen interval. The observed head from a full-screen well reaches ergodicity earlier than the head observed at a point. However, spatial averaging is not necessarily the same as the ensemble averaging.

3.3. Cross correlation analysis

The cross correlation analysis of observed head at one location and heterogeneity of hydraulic properties has been widely used in geostatistical inverse modeling (Kitanidis, 1995; Yeh et al., 1996). It is the sensitivity analysis casted in a stochastic framework. It includes not only the sensitivity, but also the spatial correlation of parameters to describe the information about the heterogeneity based on head observations. Multiplying f_j or p_j and then taking expectation on both sides of Eq. (9), we can obtain the cross-covariance ($E_{\xi f}(\mathbf{x}_0, t; \mathbf{x}_j)$ or $E_{\xi p}(\mathbf{x}_0, t; \mathbf{x}_j)$) between the observation at $\mathbf{x}_0$ and time t and the parameter f or p at $\mathbf{x}_j$ (Yeh and Liu, 2000):

$$E_{\xi f}(\mathbf{x}_0, t; \mathbf{x}_j) = \sum_{k=1}^{N} \frac{\partial \xi(\mathbf{x}_0, t)}{\partial f(\mathbf{x}_k)} C(\mathbf{x}_k, \mathbf{x}_j);$$

$$E_{\xi p}(\mathbf{x}_0, t; \mathbf{x}_j) = \sum_{k=1}^{N} \frac{\partial \xi(\mathbf{x}_0, t)}{\partial p(\mathbf{x}_k)} D(\mathbf{x}_k, \mathbf{x}_j) \quad (22)$$

The cross correlation is equal to the cross covariance normalized by the standard deviation of parameter f or s and the standard deviation of ξ (obtained by Eq. (10)).

Since spatial patterns of the cross-correlation between observed heads at an observation and heterogeneity have been well-explored in Mao et al. (2013a), Sun et al. (2013), Tso et al. (2016) and Wu et al. (2005), here we will focus on the temporal evolution of the cross-correlation. The cross-correlation analysis in this section uses the same finite element mesh as that in the analysis of previous sections.

The cross-correlation between head $h(t)$ at the observation well and ln$K$ everywhere in the domain as a function of time is plotted in Fig. 9(a). The corresponding plot between head and lnS_s everywhere versus time t is shown in Fig. 9(b). Fig. 9(a) illustrates that the correlations of head and ln$K$ at all locations are negative at the very early time ($t < 0.01$), when the cone of depression for mean flow has not reached the observation well. After that ($0.01 < t < 2$), the rapid evolutions of cross-correlations values can be divided into three groups. In group 1, negative correlations increase with time, reaching peak negative values, and then decrease with time. This group generally locates at the region between the pumping well and the observation well. In group 2, the large correlations (with negative signs) decrease with time until reaching zero and then increase with time. This group represents the two kidney shape areas near the observation well and the pumping well (see Sun et al. (2013)). The last group resides at far fields. It starts with near-zero correlations and its correlations then increase rapidly as time progresses. This implies that the information about the

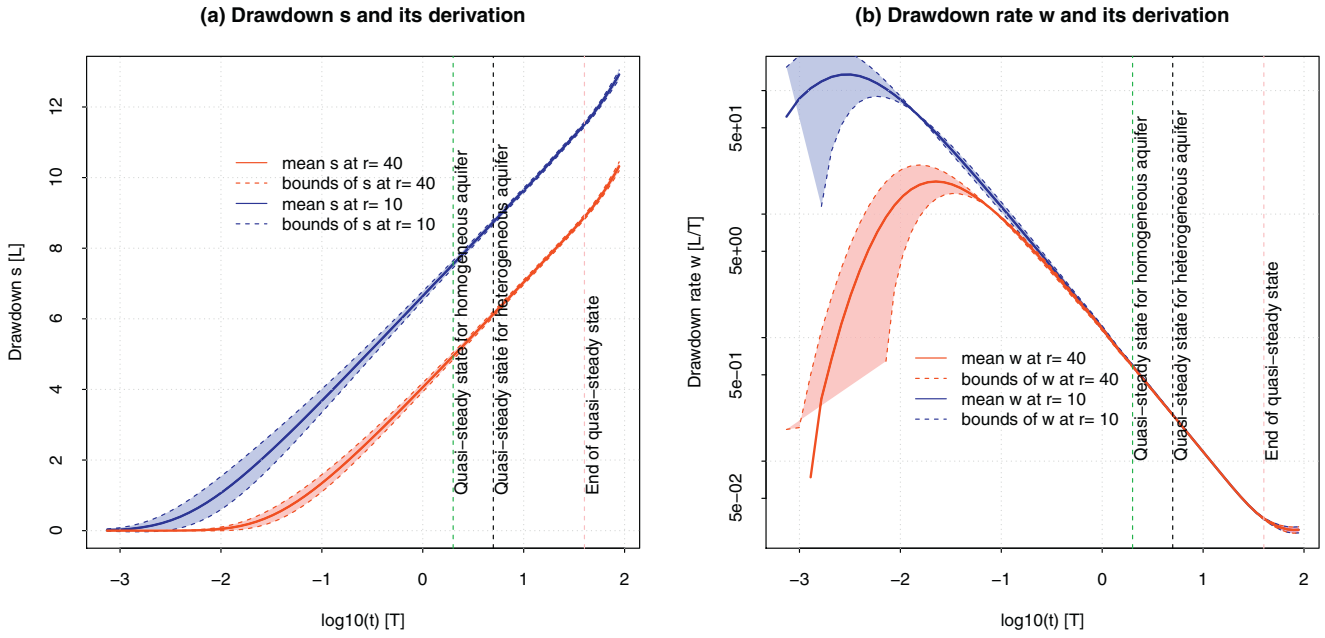

Fig. 7. The temporal evolutions of drawdown s and its derivative w at different observation locations ($r = 10$ or 40). The shadow area indicating the bounds is calculated by adding or subtracting standard derivation. Variance of $p = 1$, correlation scales are 10, 10, and 3. Variance of $f = 0$.

heterogeneity contained in the head at the observation well progressively includes heterogeneity at the far field.

The rapid change of correlations is followed by a slow temporal change ($2 < t < 40$), where the negative correlations increase gradually and the positive correlations decrease slowly. Apparently, this indicates that after the mean flow reaches quasi-steady state conditions, the information embedded in the observation tend to stabilize, although the head is still evolving. The stabilization of the correlation at quasi-steady state conditions is attributed to the stabilization of the ensemble mean hydraulic gradient. The final stage ($t > 40$) shows a change of correlation pattern, which is attributed to the effect of no-flux boundary.

Fig. 9(b) shows that the cross-correlation between head and $\ln S_s$ at all locations increases with time to a peak value, and then decreases gradually until the drawdown reaches the no-flux boundary. After this time ($t > 40$), the correlation of head and $\ln S_s$ increases again. It should be noted that the time to reach the peak value varies with location. The one closer to the pumping well, the earlier it reaches the peak value. This behavior is mainly dictated by the evolution of the drawdown rate w.

These results are consistent with the findings of Sun et al. (2013). One important finding in this paper is that, although the system does not reach steady state, the cross-correlations between head observations stabilize after the establishment of quasi-steady state, and they evolve after the drawdown reaches the boundary. This behavior indicates that during quasi-steady regime, the head observation at a well contains highly-correlated (or redundant) information. We thus recommend utilizing the early-time data in inverse models (such as HT). While the head observations at the observation well during quasi-steady regime have experienced many heterogeneities, heterogeneities at different locations at far field contributes equally and marginally to the head observation. Since there are no observation wells at the far field, the observations can improve the estimates of the mean parameters (Wen et al., 2010; Wu et al., 2005). However, if the aquifer has large-scale trends of heterogeneity, after the flow reaches the boundary or the anomaly, the quasi-steady will be interrupted and the head observations will be useful again to detect the far-field heterogeneity (Sun et al., 2013).

4. Field evidence

We examine the issues discussed above using a large number of drawdown-time data collected from an HT survey conducted at the North Campus Research Site (NCRS) on the University of Waterloo campus, in Waterloo, Ontario, Canada (Berg and Illman, 2011). The field site is an interlobate feature composed of kettle and kame deposits containing alternating layers of till and glaciofluvial material. The main features of the site are the two high K aquifers separated by a discontinuous low K unit. The upper aquifer is composed of sand to sandy silt, while the lower aquifer is composed of sandy gravel. The low K unit separating the two aquifers is discontinuous and can possibly provide hydraulic connection (Alexander et al., 2011). Above and below the aquifer zone are low K silts and clays. Detail geology can be found in Alexander et al. (2011).

Based on previous pumping tests performed at the site (Alexander et al., 2011), the aquifer at the NCRS behaves as a confined aquifer. Alexander et al. (2011) performed 471 permeameter tests and 270 grain size analyses to produce a detailed K profile along these boreholes. Furthermore, slug and pumping tests were performed to estimate K along these boreholes. They estimated that $\ln K$ had a vertical correlation length of 0.15 m and a variance of 6.50. Berg and Illman (2011) estimated that the $\ln K$ has an isotropic horizontal correlation scale of 4.0 m. The $\ln S_s$ is assumed to have the same correlation scales as $\ln K$, but the variance is 1.0, which is smaller than that of $\ln K$. The mean K and S_s values are 8×10^{-6} m/s and 1×10^{-4} m^{-1}, respectively.

There are a total number of nine wells, including four multilevel CMT wells, containing seven observation ports, and five multilevel pumping wells (PW) that each consisted of three to five ports. The nine wells are distributed in a 15×15 m squared area (Berg and Illman, 2011). For the CMT wells, the screens were spaced 2-m apart with the upper most screens located between 4.5 and 5.5 m below-ground surface, and the deepest screens were set at 16.5 to 17.5 m below ground surface. Nine pumping tests were conducted at different locations and with different constant rates (ranging from 1.5 to 30.2 L/min and lasting for 6–22.5 h) and during each pumping test, head data were collected at 27 to 38 observations ports (Berg and Illman, 2011). Therefore, 280 drawdown-time curves are

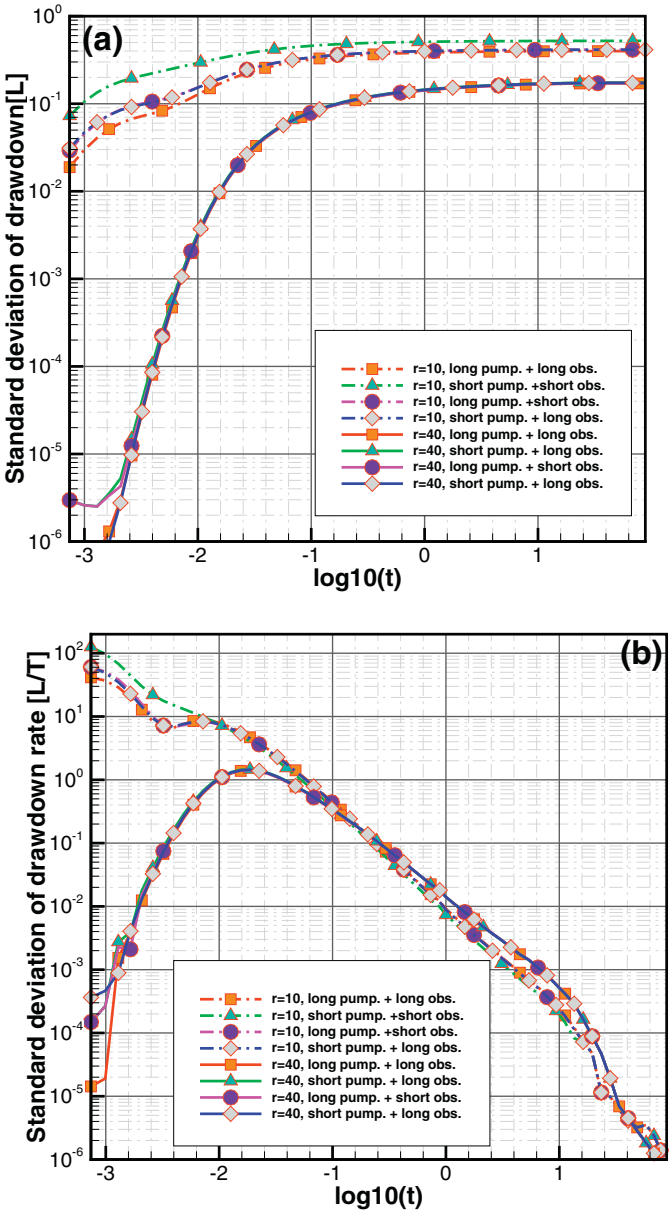

Fig. 8. The influences of well screen length on the variablity of drawndwon s (a) and its time derivative w (b) introduced by heterogeneity of K. The variablities are measured by the standard deviations of s or w. Variance of $f=1$, correlation scales are 10, 10, and 3. Variance of $p=0$.

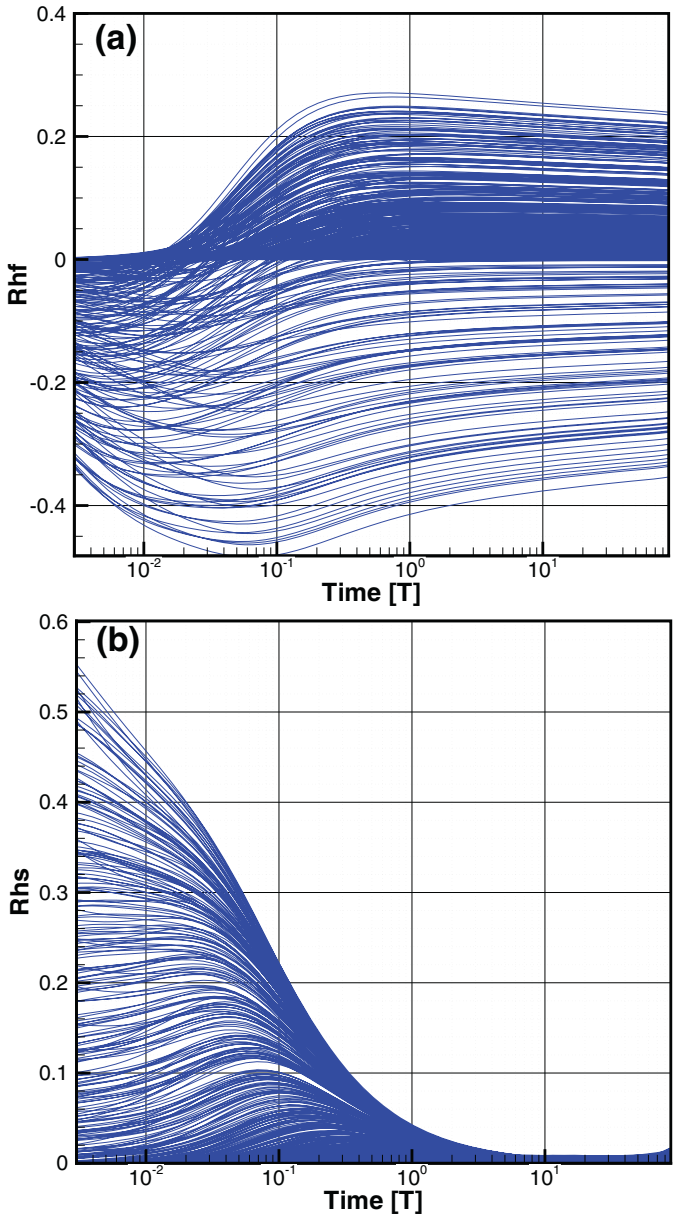

Fig. 9. The temporal evolution of correlations between hydraulic head $h(t)$ at the observation well and parameter (a) $\ln K$ or (b) $\ln S_s$ everywhere versus time t. In both case, the variance is 1 and correlation scales are 10, 10, and 3.

available to examine the variability of the flow fields induced by pumping tests at this site. The temporal interval of records ranges from 1 to 10 s. The distances r between pumping and observation wells are 3∼15 m. To eliminate the influences of pumping rate and r in the analysis, drawdown is normalized by pumping rate Q and t is normalized by r^2.

Fig. 10 presents the mean and bounds (standard deviations) of the temporal evolutions of the 280 drawdown-time data (Fig. 10(a)) and their drawdown derivative (Fig. 10(b)). Individual drawdown and its derivative w are presented in gray lines. The mean is calculated by simple arithmetic averaging of these gray lines. When the number of the drawdown derivative curves is insufficient, it is recommended to use the averaging method proposed by Lu and Stauffer (2012). It should be noted that those drawdown data from nine cross-hole tests during the HT are normalized by their pumping rates and t is normalized by r^2 (i.e., $t'=t/r^2$), where r is the distance between pumping and observation wells for each curve. The drawdown derivative is calculated by taking derivative of the normalized drawdown with respect to t' . Overall, the data tell us that at NCRS site, the variability of w exists throughout the pumping duration. That is, no quasi-steady conditions are observed. This result corroborates our stochastic analysis, and it suggests that the NCRS site likely is highly heterogeneous, and approximate quasi-steady conditions exist only in the ensemble mean sense. Nevertheless, these conditions have not developed since the pumping tests last only approximately 10,000 s.

To further explain the large variability of w at this site, the drawdown and corresponding temporal derivative induced by pumping test conducted at PW1-3 is plotted in Fig. 11. Here t is normalized by r^2. It shows a similar behavior as those in Fig. 10, although the mean drawdown shows abnormal rise due to insufficient curves at late time. Examining drawdown responses at

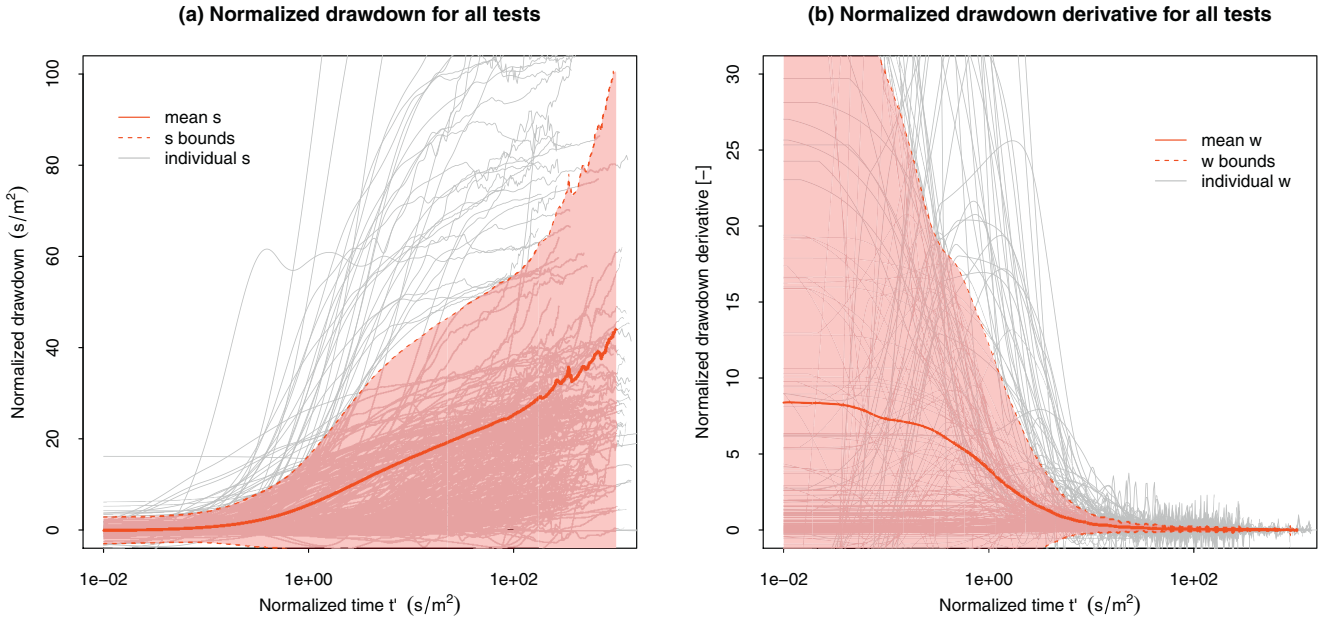

Fig. 10. The temporal evolutions of drawdown s, its derivative w and their bounds (adding or extracting one standard deviation) collected in nine pumping tests conducted at the NCRS site. Red solid line is the mean value calculated from 280 curves at different observation points. Drawdown data are normalized by their pumping rates and the horizontal axis $t' = t/r^2$ is normalized by r^2. (For interpretation of the references to colour in this figure legend, the reader is referred to the web version of this article.)

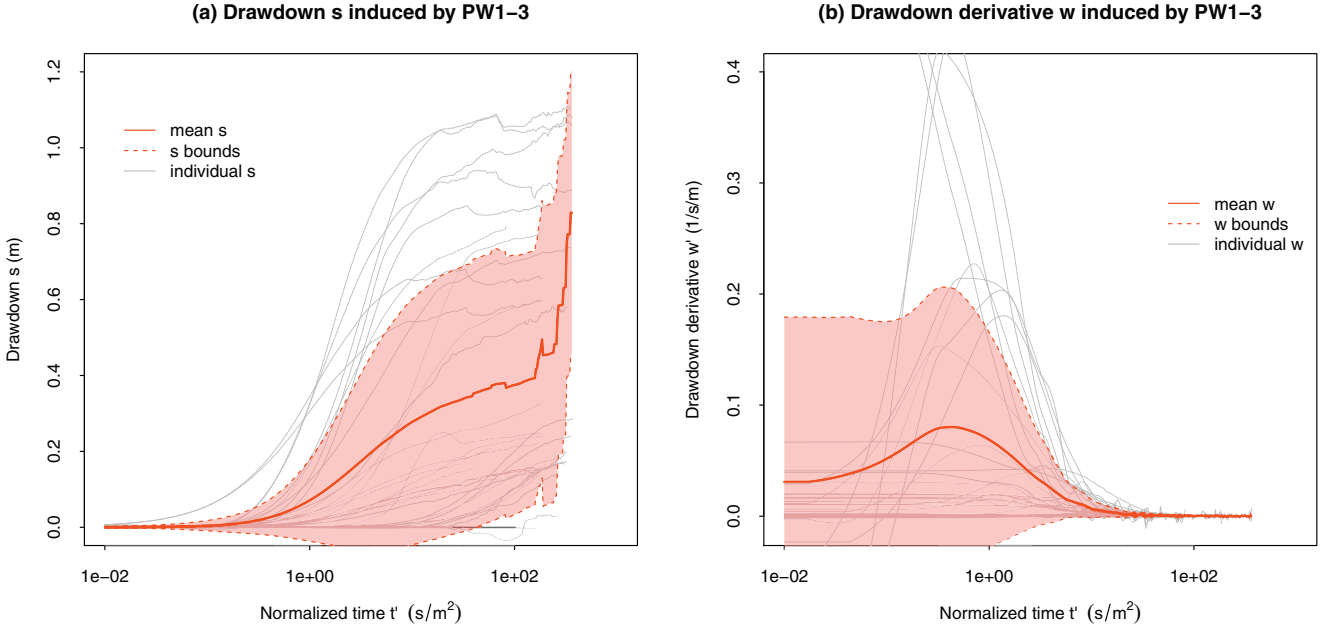

Fig. 11. The temporal evolutions of drawdown s and its derivative w during the pumping test conducted at PW1-3 at the NCRS site. The horizontal axis $t' = t/r^2$ is normalized by r^2.

different depths and locations, we find that when the observation locations and pumping location PW1-3 are well connected, the drawdown responses tend to be very quick and strong. On the other hand, observation responses in low-permeable layers are very small and slow, some of which still grow even when other locations reach approximate steady state conditions (see Fig. 9.7 in Yeh et al. (2015b)). These findings corroborate well with our stochastic analysis and the statement in Vasco and Karasaki (2006) that the kick off time of quasi-steady conditions may be delayed by the presence of low-conductivity regions (heterogeneity) where drawdowns fail to equilibrate with those in the surrounding medium. Once again, quasi-steady or steady shape exists only in the ensemble sense.

At last, Fig. 12 shows the C_w of the observed data at the site as a function of time. The C_w is obtained by normalizing the standard deviation calculated from the 280 drawdown-rate versus time curves with their mean. The green line is calculated by 1-exp(-u) with $u = r_m^2 S_s/(4Kt)$, which denotes the maximum relative differences of w for all the observations from different locations with $r_m = 15$ m, $K = 8 \times 10^{-6}$ m/s and $S_s = 1 \times 10^{-4}$ m^{-1}. If the aquifer is homogenous, the green line should be the upper bound of the calculated C_w obtained from a limited number of wells. However, the calculated C_w exceeds the green line after $t' > 3$ or $t > 675$ s, indicating strong heterogeneity of the site. Notice that the pattern of the C_w here is not the same as those from numerical stochastic analysis. Three possible reasons are listed. (1) The calculated

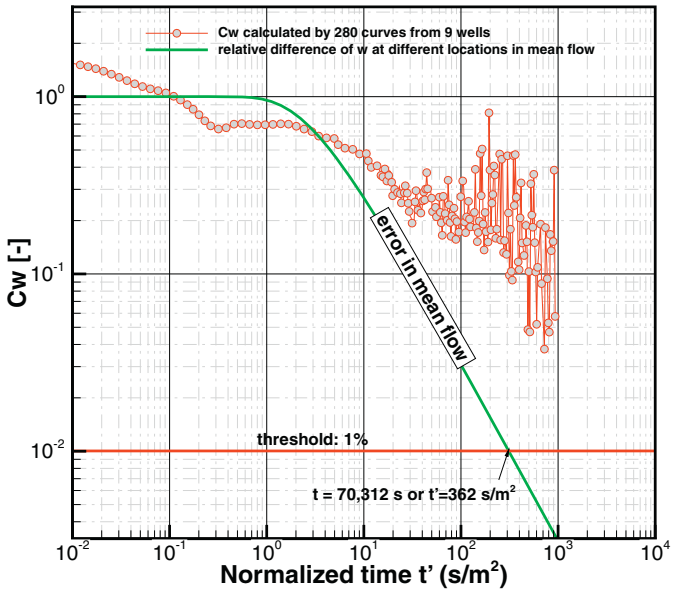

Fig. 12. Coefficient of variation C_w (defined by standard deviation of w normalized by w) versus time calculated by the 280 drawdown-time curves collected at NRCS site. The horizontal axis $t' = t/r^2$ is normalized by r^2. The green line is 1-exp(-u) indicating the relative error of w in the mean flow according to Eq. (3). (For interpretation of the references to colour in this figure legend, the reader is referred to the web version of this article.)

variability by spatial averaging is not representative to resemble ensemble variance since there are only a finite number of pumping tests and observation wells. (2) Due to the short durations of the pumping events, the flow has not reached the ergodicity condition and thus the calculated C_w by spatial averaging is not representative, especially at the early time and late time. (3) The first-order approximation may introduce error in the numerical analysis.

Based on the first two reasons, one questions the reliability of the estimated geostatistical parameters using the drawdown rate data collected from few observations wells, such as Copty and Findikakis (2004), Neuman et al. (2004) and Zech et al. (2015). Of course, if the flow reaches quasi-steady conditions in a heterogeneity aquifer, the data are likely sufficient in time for the analysis. However, sparse spatial samples likely limit the representativeness of the estimates. For this reason, data fusion techniques (e.g., geostatistical inverse model combined with HT survey, see Yeh et al. (2015a,b)) is deemed necessary to characterize detailed heterogeneity at a field site. Detailed information about heterogeneity is always useful for reliable flow and transport predictions.

5. Summary and conclusions

A quantitative definition of the quasi-steady condition during a pumping test is given in this study for 2-D and 3-D flow in homogenous, unbounded aquifers. That is, if the relative difference of w (rate of change in head) at different locations in an unbounded equivalent homogeneous aquifer is less than 1%, the concentric cone of depression at that time is considered to reach a quasi-steady condition in an approximate sense. Subsequently, we investigate its validity in bounded, heterogeneous aquifers, where K and S_s are considered as random fields. We then present 280 drawdown-time curves observed at 48 locations during nine pumping tests in a field to discuss the existence of onset time for quasi-steady state conditions of the cone of depression in real-world situations.

Based on our analysis, the following general conclusions are drawn:

(1) In a two-dimensional, homogeneous, unbounded aquifer, quasi-steady conditions exist in an approximate sense. Although drawdown s increases logarithmically with t and never attains a steady state, the flux or head gradient can be approximately regarded as a sole function of r within a circular quasi steady-state region, and the area of region expand linearly with t.

(2) For partially-screened pumping wells in three-dimensional homogeneous aquifers, the drawdown at nearby wells first behaves as 3-D flow and then transits to 2-D flow if the aquifer is thin. Once the cone of depression reaches impermeable boundaries (i.e., large-scale heterogeneity), the quasi-steady conditions vanish. If it reaches constant head boundaries, the flow becomes steady.

(3) In heterogeneous aquifers, we find that large correlation scale and large variance of hydraulic conductivity lead to large variation of w (the rate of change in head), and this variation does not vanish before the mean flow reaches steady state. On the other hand, the variability of S_s affects the variability of drawdown or its rate only slightly but delays the time to quasi-steady state conditions.

(4) The screen length of a pumping well or an observation well affects the drawdown rate only at early time, and they have little impact on the development of quasi-steady conditions. Nonetheless, the screen length of a pumping well reduces the variability of drawdown.

(5) The cross-correlation analysis indicates that although a flow field does not reach steady state conditions, the cross-correlations between head observations at different time and ln$K$ everywhere in the aquifer stabilize after the mean flow reaches quasi-steady conditions. This result indicates that during quasi-steady regime, the head observations contain temporally highly-correlated information. While the drawdown observation after this time may carry information about heterogeneity at greater distances, this information is however hard to decipher unless observation wells are available at far distances. The cross-correlation for S_s heterogeneity decays rapidly with drawdown rate until no-flux boundary or large-scale low-permeable heterogeneity is encountered.

(6) The field data show that quasi-steady conditions have not developed over the time span of the pumping tests at NCRS site. Analysis of the C_w of the observed data at the site indicates a high degree of heterogeneity at the site, which contributes to the large deviation of drawdown responses. This finding is consistent with the result of our stochastic analysis.

The quasi-steady method for the HT analysis proposed by Bohling et al. (2002) has been shown to be useful in a field experiment with limited observations (Bohling et al., 2007). However, if the aquifer is highly heterogeneous in terms of hydraulic conductivity, the temporal derivative of the ensemble mean drawdown will be quite different from those observed at individual well at different portions of the aquifer. Consequently, different drawdown derivative values should not be treated as the same even an approximate quasi-steady may exist under some conditions, since they may provide useful information about the heterogeneity. To maximize the information embedded in the collected data, transient-based simulation approach [e.g., (Sun et al., 2013; Xiang et al., 2009; Zha et al., 2015; Zha et al., 2016; Zhu and Yeh, 2005)] is deemed to be the most appropriate, although the computational cost is higher. Nevertheless, this cost will be overcome as computational technology advances.

It should be noted that the above conclusions are qualitative in nature due to the methodology we adopted in this study.

Specifically, our study is based on the first-order approximation, which requires the aquifer heterogeneity has a small variance and a univariate distribution. These two conditions may not hold in some field situations (including the NCRS site studied here). Higher-order analyses in the future are required to further substantiate our conclusions.

Acknowledgments

The work was supported by the U.S. Environmental Security Technology Certification Program (ESTCP) grant ER-201212. Additional support partially comes from the NSF EAR grant 1014594. The first author acknowledges the supports from National Natural Science Foundation of China (No. 51609173), the open-end fund provided by Key Laboratory for Groundwater and Ecology in Arid and Semi-Arid Areas, CGS (No. KLGEAS201601), and the Special Fund for Public Industry Research from Ministry of Land and Resources of China (No. 201511047). T.-C.J. Yeh also acknowledges the Outstanding Oversea Professorship award through Jilin University from the Department of Education, China as well as the Global Expert award through Tianjin Normal University from the Thousand Talents Plan of Tianjin City. J.-C. Wen would like to acknowledge the research support from, MOST 103-2221-E-224-054, MOST 104-2221-E-224-039, and MOST 105-2625-M-224-002 by the Minister of Science and Technology, Taiwan. We thank Professor Walter Illman at the University of Waterloo for providing the field data. All the other data from this work are available upon request through the corresponding author. The suggestions from three anonymous reviewers are appreciated.

References

Alexander, M.S., Berg, J., Illman, W.A., 2011. Field study of hydro- geologic characterization methods in a heterogeneous aquifer. Ground Water 49 (3), 365–382. http://dx.doi.org/10.1111/j.1745-6584.2010.00729.x.

Anderson, M., Woessner, W., Hunt, R., 2015. Applied Groundwater Modeling. Academic Press, London.

Berg, S.J., Illman, W.A., 2011. Three-dimensional transient hydraulic tomography in a highly heterogeneous glaciofluvial aquifer-aquitard system. Water Resour. Res. 47 (10), W10507. http://dx.doi.org/10.1029/2011WR010616.

Bohling, G.C., Zhan, X., Butler, J.J., Zheng, L., 2002. Steady shape analysis of tomographic pumping tests for characterization of aquifer heterogeneities. Water Resour. Res. 38 (12), 1324. http://dx.doi.org/10.1029/2001WR001176.

Bohling, G.C., Butler, J.J., Zhan, X., Knoll, M.D., 2007. A field assessment of the value of steady shape hydraulic tomography for characterization of aquifer heterogeneities. Water Resour. Res. 43 (5), W05430. http://dx.doi.org/10.1029/2006WR004932.

Butler, J.J., 1988. Pumping tests in nonuniform aquifers — The radially symmetric case. J. Hydrol. 101 (1–4), 15–30. http://dx.doi.org/10.1016/0022-1694(88)90025-X.

Cooper, H.H., Jacob, C.E., 1946. A generalized graphical method for evaluating formation constants and summarizing well-field history. Eos. Trans. AGU 27 (4), 526–534.

Copty, N.K., Findikakis, A.N., 2004. Stochastic analysis of pumping test drawdown data in heterogeneous geologic formations. J. Hydraul. Res. 42 (S1), 59–67. http://dx.doi.org/10.1080/00221680409500048.

Dagan, G., 1982. Stochastic modeling of groundwater flow by unconditional and conditional probabilities: 1. Conditional simulation and the direct problem. Water Resour. Res. 18 (4), 813–833. http://dx.doi.org/10.1029/WR018i004p00813.

Domenico, P.A., Schwartz, F.W., 1998. Physical and Chemical Hydrogeology. John Wiley & Sons Inc, New York.

Heath, R.C., 2009. Another look at steady-shape conditions. Ground Water 47 (5), 612–614. http://dx.doi.org/10.1111/j.1745-6584.2009.00593.x.

Heath, R.C., Trainer, F.W., 1968. Introduction to Groundwater Hydrology. John Wiley & Sons, New York.

Hu, R., Brauchler, R., Herold, M., Bayer, P., 2011. Hydraulic tomography analog outcrop study: combining travel time and steady shape inversion. J. Hydrol. 409 (1–2), 350–362. http://dx.doi.org/10.1016/j.jhydrol.2011.08.031.

Huang, S.Y., Wen, J.C., Yeh, T.C.J., Lu, W., Juan, H.L., Tseng, C.M., Lee, J.H., Chang, K.C., 2011. Robustness of joint interpretation of sequential pumping tests: numerical and field experiments. Water Resour. Res. 47 (10), W10530. http://dx.doi.org/10.1029/2011WR010698.

Kitanidis, P.K., 1995. Quasi-linear geostatistical theory for inversing. Water Resour. Res. 31 (10), 2411–2419. http://dx.doi.org/10.1029/95WR01945.

Leven, C., Dietrich, P., 2006. What information can we get from pumping tests?-comparing pumping test configurations using sensitivity coefficients. J. Hydrol. 319 (1–4), 199–215. http://dx.doi.org/10.1016/j.jhydrol.2005.06.030.

Lu, Z., Stauffer, P.H., 2012. On estimating functional average breakthrough curve using time-warping technique and perturbation approach. Water Resour. Res. 48 (5), 1–11. http://dx.doi.org/10.1029/2011WR011506.

Lu, Z., Vesselinov, V.V., 2015. Analytical sensitivity analysis of transient groundwater flow in a boundedmodel domain using the adjoint method. Water Resour. Res. 51 (7), 5060–5080. http://dx.doi.org/10.1016/0022-1694(68)90080-2.

Mao, D., Yeh, T.C.J., Wan, L., Lee, C.H., Hsu, K.C., Wen, J.C., Lu, W., 2013a. Cross-correlation analysis and information content of observed heads during pumping in unconfined aquifers. Water Resour. Res. 49 (2), 713–731. http://dx.doi.org/10.1002/wrcr.20066.

Mao, D., Yeh, T.C.J., Wan, L., Hsu, K.C., Lee, C.H., Wen, J.C., 2013b. Necessary conditions for inverse modeling of flow through variably saturated porous media. Adv. Water Resour. 52, 50–61. http://dx.doi.org/10.1016/j.advwatres.2012.08.001.

Neuman, S.P., Guadagnini, A., Riva, M., 2004. Type-curve estimation of statistical heterogeneity. Water Resour. Res. 40, W04201. http://dx.doi.org/10.1029/2003wr002405.

Neuman, S.P., Blattstein, A., Riva, M., Tartakovsky, D.M., Guadagnini, A., Ptak, T., 2007. Type curve interpretation of late-time pumping test data in randomly heterogeneous aquifers. Water Resour. Res. 43 (10), W10421. http://dx.doi.org/10.1029/2007WR005871.

Pedretti, D., Russian, A., Sanchez-Vila, X., Dentz, M., 2016. Scale dependence of the hydraulic properties of a fractured aquifer estimated using transfer functions. Water Resour. Res. 52 (7), 5008–5024. http://dx.doi.org/10.1002/2016WR018660.

Pedretti, D., Fiori, A., 2013. Travel time distributions under convergent radial flow in heterogeneous formations: Insight from the analytical solution of a stratified model. Adv. Water Res. 60, 100–109. http://dx.doi.org/10.1016/j.advwatres.2013.07.013.

Renard, P., Glenz, D., Mejias, M., 2009. Understanding diagnostic plots for well-test interpretation. Hydrogeol. J. 17 (3), 589–600. http://dx.doi.org/10.1007/s10040-008-0392-0.

Sanchez-Vila, X., Tartakovsky, D.M., 2007. Ergodicity of pumping tests. Water Resour. Res. 43 (3), W03414. http://dx.doi.org/10.1029/2006WR005241.

Schneider, C.L., Attinger, S., 2008. Beyond Thiem : a new method for interpreting large scale pumping tests in heterogeneous aquifers. Water Resour. Res. 44, 1–14. http://dx.doi.org/10.1029/2007WR005898.

Srivastava, R., Yeh, T.C.J., 1992. A three-dimensional numerical model for water flow and transport of chemically reactive solute through porous media under variably saturated conditions. Adv. Water Resour. 15 (5), 275–287. http://dx.doi.org/10.1016/0309-1708(92)90014-S.

Straface, S., Yeh, T.C.J., Zhu, J., Troisi, S., Lee, C.H., 2007. Sequential aquifer tests at a well field, Montalto Uffugo Scalo, Italy. Water Resour. Res. 43 (7), W07432. http://dx.doi.org/10.1029/2006WR005287.

Sun, R., Yeh, T.C.J., Mao, D., Jin, M., Lu, W., Hao, Y., 2013. A temporal sampling strategy for hydraulic tomography analysis. Water Resour. Res. 49 (7), 3881–3896. http://dx.doi.org/10.1002/wrcr.20337.

Thiem, G., 1906. Hydrologische Methoden. J.M. Gebhardt, Leipzig.

Theis, C.V., 1935. The relation between the lowering of the Piezometric surface and the rate and duration of discharge of a well using ground-water storage. Trans. Am. Geophys. Union 16 (2), 519–524. http://dx.doi.org/10.1029/TR016i002p00519.

Tso, C.H.M., Zha, Y., Yeh, T.C.J., Wen, J.C., 2016. The relative importance of head, flux, and prior information in hydraulic tomography analysis. Water Resour. Res. 52 (1), 3–20. http://dx.doi.org/10.1002/2015WR017191.

Vasco, D.W., Karasaki, K., 2006. Interpretation and inversion of low-frequency head observations. Water Resour. Res. 42 (5), W05408. http://dx.doi.org/10.1029/2005WR004445.

Wen, J.C., Wu, C.M., Yeh, T.C.J., Tseng, C.M., 2010. Estimation of effective aquifer hydraulic properties from an aquifer test with multi-well observations (Taiwan). Hydrogeol. J. 18 (5), 1143–1155. http://dx.doi.org/10.1007/s10040-010-0577-1.

Wu, C.M., Yeh, T.C.J., Zhu, J., Lee, T.H., Hsu, N.S., Chen, C.H., Sancho, A.F., 2005. Traditional analysis of aquifer tests: comparing apples to oranges? Water Resour. Res. 41 (9), W09402. http://dx.doi.org/10.1029/2004WR003717.

Xiang, J., Yeh, T.C.J., Lee, C.H., Hsu, K.C., Wen, J.C., 2009. A simultaneous successive linear estimator and a guide for hydraulic tomography analysis. Water Resour. Res. 45 (2), W02432. http://dx.doi.org/10.1029/2008WR007180.

Yeh, T.C.J., Mao, D., Zha, Y., Wen, J.C., Wan, L., Hsu, K., Lee, C., 2015a. Uniqueness, scale, and resolution issues in groundwater model parameter identification. Water Sci. Eng. 8 (3), 175–194. http://dx.doi.org/10.1016/j.wse.2015.08.002.

Yeh, T.C.J., Khaleel, R., Carroll, K.C., 2015b. Flow Through Heterogeneous Geologic Media. Cambridge University Press, Cambridge.

Yeh, T.C.J., Lee, C.H., 2007. Time to change the way we collect and analyze data for aquifer characterization. Ground Water 45 (2), 116–118. http://dx.doi.org/10.1111/j.1745-6584.2006.00292.x.

Yeh, T.C.J., Liu, S., 2000. Hydraulic tomography: Development of a new aquifer test method. Water Resour. Res. 36 (8), 2095–2105. http://dx.doi.org/10.1029/2000WR900114.

Yeh, T.C.J., Jin, M., Hanna, S., 1996. An iterative stochastic inverse method: conditional effective transmissivity and hydraulic head fields. Water Resour. Res. 32 (1), 85–92. http://dx.doi.org/10.1029/95WR02869.

Zech, A., Arnold, S., Schneider, C., Attinger, S., 2015. Estimating parameters of aquifer heterogeneity using pumping tests – implications for field applications. Adv. Water Resour. 83, 137–147. http://dx.doi.org/10.1016/j.advwatres.2015.05.021.

Zech, A., Attinger, S., 2015. Technical note: analytical solution for the mean drawdown of steady state pumping tests in two-dimensional isotropic heterogeneous aquifers. Hydrol. Earth Syst. Sci. Discuss. 12 (7), 6921–6944. http://dx.doi.org/10.5194/hessd-12-6921-2015.

Zha, Y., Yeh, T.C.J., Illman, W.A., Tanaka, T., Bruines, P., Onoe, H., Saegusa, H., 2015. What does hydraulic tomography tell us about fractured geological media? A field study and synthetic experiments. J. Hydrol. 531 (1), 17–30. http://dx.doi.org/10.1016/j.jhydrol.2015.06.013.

Zha, Y, Yeh, TCJ, Illman, WA, Tanaka, T, Bruines, P, Onoe, H, Saegusa, H, Mao, D, Takeuchi, S, Wen, JC, 2016. An application of hydraulic tomography to a large-scale fractured granite site, Mizunami, Japan. Groundwater 54 (6), 793–804. http://dx.doi.org/10.1111/gwat.12421.

Zhang, J., Yeh, T.C.J, 1997. An iterative geostatistical inverse method for steady flow in the vadose zone. Water Resour. Res. 33 (1), 63–71. http://dx.doi.org/10.1029/96WR02589.

Zhu, J., Yeh, T.C.J., 2005. Characterization of aquifer heterogeneity using transient hydraulic tomography. Water Resour. Res. 41, 1–10. http://dx.doi.org/10.1029/2004WR003790.